NATIONAL RADIO ASTRONOMY OBSERVATORY
CHARLOTTESVILLE, VIRGINIA

ELECTRONICS DIVISION INTERNAL REPORT NO. 268

SIS MIXERS AT 115 GHz USING Nb/Al -Al_2O_3/Nb JUNCTIONS

S.-K PAN, A. R. KERR, J. W. LAMB
AND
M. J. FELDMAN*

APRIL 1987

* DEPARTMENT OF ELECTRICAL ENGINEERING, UNIVERSITY OF VIRGINIA, CHARLOTTESVILLE, VA 22901.

NUMBER OF COPIES: 150

SIS MIXERS AT 115 GHz USING Nb/Al-Al_2O_3/Nb JUNCTIONS

S.-K. Pan, A. R. Kerr, J. W. Lamb and M. J. Feldman

TABLE OF CONTENTS

SIS MIXERS AT 115 GHz USING Nb/Al-Al_2O_3/Nb JUNCTIONS

S.-K. Pan, A. R. Kerr, J. W. Lamb and M. J. Feldman

ABSTRACT

This report describes measurements at ~ 115 GHz on SIS mixers using Nb/Al-Al_2O_3/Nb junctions fabricated by Hypres Inc. Operated at 2.5 K, the mixer conversion loss was as low as 4.6 dB SSB, with a mixer noise temperature of 16 K SSB, giving an overall receiver noise temperature of 82 K SSB at the room-temperature feed horn. At an operating temperature of 4.2 K, the receiver noise temperature increased to 96 K. These mixers are now in use on the NRAO 12-m Kitt Peak telescope.

Measurements of saturation power and bandwidth are described. Self-heating effects are evident in some junctions, but do not appear to degrade the mixer performance. Analysis of the mixer performance supports the value of 60 $fF/\mu m^2$ for the specific capacitance of these junctions.

Some of the mixers contained an inductive loop (stub) to tune out the capacitance of the SIS array. The consistently poor performance of these mixers was found to be a result not only of the larger than expected specific capacitance of the junctions, but also of the parasitic series inductance of the array. These factors limit the usefulness of this type of tuning structure.

SIS MIXERS AT 115 GHz USING Nb/Al-Al_2O_3/Nb JUNCTIONS

S.-K. Pan, A. R. Kerr, J. W. Lamb and M. J. Feldman

I. Introduction

In the past few years, the superconductor-insulator-superconductor (SIS) quasi-particle tunnel-junction mixer has been recognized as the best choice for use in low-noise millimeter-wave receivers [1]. This is a result of the extremely low shot-noise, low LO power requirement, and potential conversion gain of SIS mixers. Currently, about ten SIS receivers, operating from 45 to 230 GHz, have been reported in use on radio telescopes around the world, although most of these have sensitivities no better than their main competitor, the Schottky-diode mixer receiver [1]. Until now, all of these SIS receivers have been based on lead-alloy junctions, which must be operated at ~ 2.5 K to achieve good performance. Since lead-alloy junctions are vulnerable to electric shock, heating, humidity, and possibly the mechanical stresses induced during thermal cycling, the failure rate of lead-alloy SIS mixer is unfortunately high. Certainly, their reliability is likely to be a serious consideration for a multi-receiver telescope or the proposed national millimeter array [2].

Recently, we have tested several Nb/Al-Al_2O_3/Nb SIS mixers at ~ 115 GHz. The junctions were designed by us and fabricated by Hypres, Inc. under an N.R.L. contract (see Acknowledgements). Our preliminary results are very encouraging: these junctions give excellent results, better than any lead-alloy junctions we have ever tested; they are very reliable and can be operated at 4.2 K with little loss of sensitivity. Thus they appear very suitable for practical receiver applications.

This report presents the results of our measurements. Section II contains a description of the test receiver and the method of measurement. The results of the measurements are presented in section III. In the same section, we also describe some unique characteristics which are associated with these Nb-based junctions and discuss their effects on mixer performance. Some limitations of SIS arrays with integral inductive tuning elements are described in Appendix B. The performance of these mixers in the 12-m telescope receiver (as opposed to our laboratory test receiver) is described in Appendix D.

II. Experimental Set-Up and the Method of Measurement

A. Mixer Mount

The SIS junctions were tested using the NASA/GISS type-D mixer mount [3,4], shown in Fig. 1. This mixer mount contains two adjustable backshorts which can provide the junction with almost any value of embedding admittances at a given frequency. A detailed description of the mixer mount is given in [4].

B. Test Receiver

In order to evaluate the properties of the mixer, a specially designed test receiver was used. The dewar is a modified Infrared Laboratories' model HD-3(8) which consists of a liquid nitrogen cooled radiation shield and a liquid helium cooled cold stage. The basic configuration of this receiver is very similar to that described in Ref. [4]. A photograph and simplified diagram of the receiver are shown in Fig. 2. A four-position coaxial switch (modified Dynatech/U-Z, Model M4-413C901), an L-band circulator and an isolator (Pamtech, Models 1102 and 1141), a 1-2 GHz 20 dB directional coupler (Omni Spectra, Model 2023-6123-20), and a GaAs-FET amplifier are all mounted in vacuum on the liquid helium cold-plate. The amplifier is an NRAO L-band unit as described in Ref. [5], operated with low power dissipation, which reduces its bandwidth and input return loss and increases its noise temperature a few degrees. As described later in this section, this arrangement allows us to determine the conversion loss and noise temperature of the mixer entirely from noise measurements. The four positions of the switch allow the IF amplifier to be connected to : 1) the output port of the mixer; 2) a short circuit termination; 3) a 50 ohm load which is always maintained at the bath temperature; and 4) another 50 ohm load which can be heated to 20 K.

The input waveguide and window, mixer backshort mechanism, temperature monitoring system, and the junction bias circuit, are described in detail in Ref. [4]. The noise temperature of this test receiver is expected to be 10-20 K higher than the similar receivers optimized for low-noise astronomical observations.

C. Measurement Method

The receiver can be tuned for either double sideband or single sideband response [4]. In either case, the intrinsic receiver noise temperature T_R', referred to the input port of the mixer, can be related to the conversion loss L_C, and the noise temperature T_M of the mixer through the following equation:

$$T_R' = L_C \cdot T_{IF} + T_M \qquad (1)$$

where T_{IF} is the equivalent noise temperature of the IF system. This is true provided that T_R', T_M and L_C are all either single sideband or double sideband values. Since T_R' and T_{IF} are linearly related, L_C and T_M of the mixer can be determined from measuring T_R' for several known values of T_{IF}. Our method is a variation of that proposed by Trambarulo & Berger [6].

In our test receiver, T_{IF} can be changed by injecting IF noise through the directional coupler toward the FET amplifier. The effective T_{IF}, measured at the input of the coaxial switch, is determined from a Y-factor measurement by switching the input of the FET amplifier between the 20 K heated load and the 4 K load. Using this method, T_{IF} can be measured with an accuracy better than 0.5 K. This set-up also allows us to measure the effective noise temperature of the IF section at different IF bandwidths. The measured results are presented in Table I. We found that over a period of about two months, during which the receiver was cooled many times, the IF noise temperature increased slightly from 12 K to 13.6 K (in a 25 MHz band at 1400 MHz). This shows the need for periodic remeasurement of T_{IF}.

The external receiver noise temperature T_R is measured using room temperature and 77 K black bodies in front of the room temperature feed horn. Since the insertion loss between the horn and the mixer (0.6 dB, measured) and the effective noise temperature of this section (25 K, estimated) are known [7], the intrinsic receiver noise temperature, referred to the input of mixer, can be deduced from the following formula:

$$T_R' = (T_R - 25) / 1.15 \qquad (2)$$

Since T_R is linearly related to T_{IF}, the plot of T_R' against T_{IF} is a straight line with a slope given by mixer's conversion loss. The intersection of this straight line with the $T_{IF} = 0$ axis is the mixer noise temperature. Using this method, L_C and T_M can be determined with an accuracy better than 0.2 dB and 5 K, respectively. Furthermore, in this set up, depending on the switch setting, a CW signal or noise can be injected through the circulator towards either the mixer's output port or the short circuit termination. By comparing the power reflected from these two, the mixer's IF mismatch can be determined.

III. Results and Discussion

A. Junction Design

Several wafers with different current densities have been supplied by Hypres, Inc. Each wafer is 2 in. diameter and contains 26,400 different mixer cells. Some of these cells are shown in Fig. 3 and similar pictures of our junctions were published without acknowledgement in [8]. There are a total of 72 different designs for 115 GHz, with several different junction sizes, number of junctions in series, and tuning inductances. Arrays with 1, 2, 4, or 10 junctions were designed with junction sizes varying from 1.5 x 1.5 to 3.75 x 3.75 microns. The RF tuning circuit consists of a two-wire transmission line stub, i.e., inductive loop, in parallel with the SIS array. The loop is broken by a pair of blocking capacitors to provide an IF and dc block. Because of fabrication uncertainties, five different values of the inductive loop were included. It was expected that one inductance value would tune out the junction capacitance at the signal frequency such that a wide RF bandwidth could be obtained.

B. Preliminary Experiments

The first few wafers delivered by Hypres, Inc. showed poor dc I-V characteristics with $V_m(2mV)^*$ ranging from 5 to 20 mV. Most of them showed excessive leakage current just below the gap voltage. "Current bumps" above the gap voltage were also common features on the I-V curves of these junctions. A typical dc I-V curve of a four-junction series array is shown in Fig. 4. The mixing performance of these junctions was very poor. When operated at 2.5 K, the best SSB receiver noise temperature was around 220 K at 112.5 GHz.

---

* $V_m(2mV) = I_J.2mV/i(2mV)$, where $i(2mV)$ is the current at 2 mV, and I_J is the maximum dc Josephson current.

The RF tuning circuit did not operate as we had expected. The first cause of this was that the circuits had been designed assuming the specific capacitance (C_s) of the junctions was 30 fF/μm^2, the value quoted by Hypres. RF measurements led us to suspect an error in this number. These measurements, described in Appendix A, were on junctions without inductive tuning and are consistent with a mixer analysis using Tucker's theory [9] if the specific capacitance is assumed to be approximately 60 fF/μm^2, which happens to be the value measured by Gurvitch, et al. [10] for similar junctions. However, more accurate measurements are needed to determine conclusively the C_s of Nb/Al-Al_2O_3/Nb junctions and the extent to which C_s depends on critical current density and the base and counter electrode quality.

A more serious problem was identified. A detailed analysis of the RF tuning circuit using a scale model indicates that the small series inductance associated with an array of closely spaced junctions can have a profound effect on the operation of the circuit. This inductance is inside the tuning loop and can cause a large impedance transformation between the junctions and the rest of the circuit. As shown in Appendix B, the transformed value of the junction resistance can be many times lower than the actual junction resistance, especially if the junction capacitance is large. This appears to be a fundamental limitation of this type of tuning circuit.

C. Wafer WN430 - Results and Discussion

The most recent Hypres wafer (WN430) is of much higher quality. The current density of this wafer is about 1,400 A/cm^2, and V_m(2mV) is typically 40 mV at 4.2 K. Assuming C_s = 60 fF/μm^2, the junction overlap specific capacitance C_o = 3 fF/μm^2, and array resistance around 40 to 60 ohm, the effective $\omega R_N C$ product of these junctions is from 4.0 to 7.5 at 115 GHz. Fig. 5(a) shows a typical dc I-V curve at 4.2 K for an array of (nominally) 2.5 μm square junctions. Even at 4.2 K, the unpumped dc I-V curve shows an extremely steep current rise at the gap voltage. The large value of V_m(2mV) ~ 40 mV signifies that the leakage current is extremely small.

A significant difference between the present Nb junctions and earlier junctions, both Nb and Pb-alloy, is in the ratio of the resistance at room temperature to the normal resistance at 4.2 K. For all the earlier junctions (Nb and Pb-alloy) the resistance measured at room temperature was roughly equal to the normal state tunneling resistance at 4.2 K (measured at 4 mV). In the case of the present junctions, we have found that the junction resistance at room temperature is about 20% higher than at 4.2 K. This might indicate that the resistivity of the niobium films wafer is much higher than the bulk value. The reason for this anomaly is not known.

The latest wafer was made with the same mask set as before. Therefore, the RF tuning circuits are not usable and only those arrays without the inductive tuning loop have been tested. The pumped dc I-V curves show very distinct photon step structures with voltage periodicity $N\hbar\omega/e$. By adjusting the two backshort settings and the LO power, it is possible to obtain an infinite differential resistance on the first photon step below the gap, as shown in Fig. 5(b). From past experience we have found this to be a prerequisite for a good mixer. Table II summarizes the mixing properties of these junctions and the complete receiver

performance, at both 4.2 K and 2.5 K. The best results with the mixer tuned for DSB and SSB operation were obtained with the mixer operated at 2.5 K. Then L_C(SSB) = 4.6 dB, T_M(SSB) = 16 K, and L_C(DSB) = 1.8 dB, T_M(DSB) = 4 K. The corresponding receiver noise temperatures are T_R(SSB) = 82 K and T_R(DSB) = 50 K.

All of these measurements were made with the LO at 113.9 GHz and a 25 MHz IF bandwidth at 1.4 GHz.

It is very encouraging to see that, even when operated at 4.2 K, these junctions give better results than lead-alloy junctions operated at 2.5 K. Since the transition temperature T_C of niobium is quite high (~ 9.3 K), we do not expect any dramatic improvement in performance with cooling below 4.2 K. In fact, on reducing the temperature from 4.2 K to 2.5 K, the receiver noise temperature only improved by 10 to 15 K, which is much smaller than the factor of ~ 2 improvement usually seen in lead-alloy SIS receivers.

Saturation and Instantaneous Bandwidth of the Receiver

Mixer "Hypres-WN430-C5-R6-DII5" was used to measure the saturation and bandwidth properties of the receiver. The receiver saturation power, measured at the 1-dB gain compression point of the mixer, is 12.5 nW for SSB tuning and 16 nW for DSB tuning. In both cases, the saturation power is roughly 2.5 times of that calculated from the formula given by Ref. [1], eqn. 6.2. Previously, we have proposed that by biasing the junction on a non-optimum gain peak, it might be possible to increase receiver's saturation power so that we can use the receiver to look at very strong signals [2]. However, measurements show that the mixer conversion loss is best when array is biased at the first photon step below gap, and is only 3 to 6 dB worse when biased at the other steps. This result shows that the previous suggestion is impractical. However, the gain of an SIS mixer can also be reduced by changing the LO power: as the LO power is increased, a series of gain nulls occur. While operation at very low LO power would probably aggravate saturation problems due to "input saturation," operation with the LO power near one of the higher gain-nulls may give the desired increase in dynamic range. We have not yet tried this.

Fig. 6 shows the receiver's instantaneous bandwidth. In the DSB case, the receiver's noise temperature changes less than 15 K over a 400 MHz band. For the SSB case, T_R rises 35 K at the edges of a 400 MHz band. The shape of these curves is a result of the impedance and noise characteristics of the IF circuit (bias-T, circulator, isolator, coupler, and amplifier). The receiver noise temperature measured at different IF bandwidths is shown in Table III. The RF bandwidth with DSB tuning was also measured and found to be about 6 GHz.

Other Factors Affecting Mixer Performance

a) Proximity Effect

As mentioned above, the dc I-V curves of all the Hypres junctions exhibited "bump" structures above the gap voltage. This is presumably due to the proximity effect [11-13] resulting from a thin, non-superconducting Al layer right on top of the niobium base electrode. It has been a worry that this bump structure might hurt the junction's performance [14]. In our experiments, we did not observe any deleterious effect.

b) Excess Series Resistance

A small excess resistance, about 0.5 to 1 ohm, was found in series with some of the arrays. The superconducting portion of the dc I-V curve of one of such array is shown in Fig. 7. Since the Q-factor of the mixer is rather high, any parasitic series resistance can cause substantial loss. This resistance is certainly not a property of the junctions themselves, and would be of concern if it were inherent to the wafer fabrication process. Examining the SIS chip under a phase-contrast microscope, we found that junction bonding pads were partially covered by some brown material - probably remains of photoresist. Several different solvents (acetone, Toluene, TCE, and water), as well as oxygen plasma etching, were tried to remove it but failed. We are still investigating this problem.

c) Self Heating Effect

When the SIS chip was mounted in the mixer block and cooled to 4.2 K in a vacuum, junction self heating effects were observed for the larger arrays. This was particularly severe in Hypres-WN430-C5-M7-DII0, which is a ten-junction array of (nominal) 3.75 μm-square junctions. Figs. 8(a) and 8(b) shows its dc I-V curve measured in liquid helium and in a vacuum. The S-shaped I-V curve is clear evidence that the array is heated by a dc bias current of > ~ 100 μA.

We believe that this distortion of the I-V curve is caused by simple joule heating, and not by a non-equilibrium effect intrinsic to these junctions, for this following reasons:

1) The distortion largely disappears when the sample is immersed in liquid helium (Fig. 8(a)).

2) The distortion is much more severe for the larger arrays, indicating that it depends on the large-scale environment rather than microscopic effects at each junction.

3) A rough heat flow calculation for the array (see Appendix C) predicts a temperature rise of the order of 1 K. This current-dependent temperature variation would give a variation of the energy gap of the right magnitude to account for the S-shaped I-V curve [15].

4) At a larger current (~ 600 μA), the I-V curve for this array shows an abrupt jump to a higher voltage. This appears to be caused by the Nb junction interconnections going normal, and the heat flow calculation predicts the requisite temperature rise at this current.

Although the same joule heating has been observed by many authors, in particular by Huggins and Gurvitch in Nb/Al-Al_2O_3/Nb junctions [16] and by Letrou, et al. in NbN/Nb_2O_5/PbIn junctions [17], its effect on SIS mixer performance was not known. In our present measurements, it does not appear to degrade the mixer performance. In fact, this particular array gives the best mixing results of those tested (we believe this is because it has the smallest effective $\omega R_N C$ product). Nevertheless, our result may not be general, and it is important to consider the possibility of junction heating in the design of future SIS mixers.

There are several possible ways to avoid heating effects. Different substrate materials or thicker niobium films to improve heat dissipation will be tried in the future. Thermal analysis of superconducting structures is complicated by the thermal interface resistance between dissimilar materials, as described by Skocpol, et al. [18].

Possibility for High Frequency Application

Fig. 9 shows the I-V characteristic of a ten-junction array of 2.25 μm-square junctions. This is one of the arrays originally designed for 230 GHz operation. The array uniformity and dc I-V characteristic look reasonably good for this purpose. However, we do not expect good results at 230 GHz from these particular mixers because they were designed using the wrong value of specific capacitance (see section III.B), and the junction (array) series inductance discussed in section III.B will cause a large impedance transformation at 230 GHz.

To use junctions of this type at 230 GHz, a better tuning structure is needed [19] which will avoid the impedance transformation problem. Furthermore, with small junctions, the overlap capacitance between the interconnection layer and the base electrode contributes substantially to the effective $\omega R_N C$ product -- for the 2.5 μm-square Hypres junctions the overlap capacitance is 29% of the junction capacitance. This is a result of the 2-μm overlap required on each side of the junction to allow for mask alignment tolerances, and the use of an anodized niobium dielectric (Nb_2O_5, $\varepsilon_r = 30$). The overlap capacitance could be greatly reduced by using an insulating layer of SiO ($\varepsilon_r = 6$) or SiO_2 ($\varepsilon_r = 3.8$).

Junction Storage and Recyclability

These niobium junctions can be kept in the open air at room temperature without changing their characteristics. Unlike lead junctions, whose normal resistance is usually reduced by several percent each thermal cycle, the stability of these niobium junctions is extremely good. We have not detected any change in their characteristics over the eight-month experimental period. Within this period, some of the arrays have been cycled more than ten times. These properties are extremely desirable for use in practical millimeter receivers.

IV. Conclusion

Our results indicate that Nb/Al-Al_2O_3/Nb junctions are very suitable for use in radio-astronomy receivers. Two of these mixers are now in use on the NRAO 12-m telescope at Kitt Peak. With the beam splitter, polarization diplexer and lens, an SSB receiver noise temperature as low as 99 K is measured at 115.3 GHz with an instantaneous IF bandwidth of 600 MHz.

Measurements of the saturation power, bandwidth, and self-heating effects in Nb/Al-Al_2O_3/Nb mixers given in this report will be useful in designing future SIS receivers. Results reported here also provide new information on the characteristics of the Nb/Al-Al_2O_3/Nb junctions and the design of integrated tuning circuits for SIS mixers. This is valuable to the ongoing NRAO/UVA SIS junction fabrication project which is expected to produce high quality Nb/Al-Al_2O_3/Nb SIS junctions for use as mixers and detectors in the near future.

ACKNOWLEDGEMENTS

The authors gratefully acknowledge the collaboration of S. Faris, S. Whiteley, and M. Radparvar of Hypres, Inc. who fabricated the SIS junctions described in this report, and M. Nisenoff and E. Cukauskas of the Naval Research Laboratory who initiated the collaboration and have provided much support and helpful advice throughout. The work was funded through NRL Contract Nos. N00014-84-C-2212 and N00173-83-F-D112. The initial phase of the work was conducted when S.-K. P., A. R. K., and M. J. F. were at the NASA/Goddard Institute for Space Studies.

REFERENCES

1. J. R. Tucker and M. J. Feldman, "Quantum Detection at Millimeter Wavelength," Rev. of Modern Phys., vol. 57, no. 4, pp. 1055-1113, 1985.

2. S. Weinreb and A. R. Kerr, Millimeter-Array preproposal, NRAO 1986.

3. S.-K. Pan, M. J. Feldman, A. R. Kerr, and P. Timbie "Low-Noise 115-GHz Receiver Using Superconducting Tunnel Junctions," Appl. Phys. Lett., vol. 43, no. 8, pp. 786-788, Oct. 1983.

4. S.-K. Pan and A. R. Kerr, "A Superconducting Tunnel Junction Receiver for Millimeter-Wave Astronomy," NASA Technical Memorandum 87792, 7/86.

5. S. Weinreb, D. L. Fenstermacher, and R. W. Harris, "Ultra-Low-Noise, 1.2- to 1.7-GHz Cooled GaAsFET Amplifiers," IEEE Trans. Microwave Theory Tech., vol MTT-30, no 6., pp. 849, 1982.

6. R. Trambarulo and M. S. Berger, "Conversion Loss and Noise Temperature of Mixers from Noise Measurements," IEEE MTT-S Digest, pp. 364-465, 1983.

7. S.-K. Pan, (unpublished).

8. J. Barry, "SIS Mixers Drop Mm-Wave Noise Floor," Microwaves & RF, pp. 171-173, March 1986.

9. J. R. Tucker, "Quantum Limited Detection in Tunnel Junction Mixers," IEEE J. of Quantum Elec., vol. QE-15, no. 11, pp. 1234-1258, Nov. 1979.

10. M. Gurvitch, M. A. Washington, and H. A. Huggins, "High Quality Refractory Josephson Tunnel Junctions Utilizing Thin Aluminum Layers," Appl. Phys. Lett., vol. 42, no. 5, pp. 472-474, March 1983.

11. L.Y. Shen, "Superconductivity of Tantalum, Niobium and Lanthanum Studied by Electron Tunneling: Problems of the Surface Contamination," in Super conductivity in D- and F-Band Metals, edited by D.H. Douglass (Plenum, New York, 1972), pp. 31-44.

12. P. W. Wyatt, R. C. Baker, and A. Yelon, "Tunneling Study of the Superconducting Proximity Effect in the Thin Film - Normal Limit," Phys. Rev. B., vol. 6, no. 11, Dec. 1972.

13. V. Keith and J. D. Leslie, "New Technique for Electron-Tunneling Junction Fabrication and Its Application to Tantalum and Niobium," Phys. Rev. B., vol. 18, no. 9, pp. 4739-4761, Nov. 1978.

14. T. C. L. G. Sollner, private communication.

15. J. Bardeen, L. N. Cooper, and J. R. Schrieffer, "Theory of Superconductivity," Phys. Rev., vol. 108, no. 5., pp. 1175-1204, Dec. 1957.

16. H. A. Huggins and M. Gurvitch, "Preparation and Characteristics of Nb/Al-Oxide-Nb Tunnel Junctions," J. Appl. Phys., vol. 57, no. 6, pp. 2103-2109, Mar. 1985.

17. C. Letrou, D. Crete, J.-C. Pernot, A. Rabhi, and P. Encrenaz," Heterodyne Mixing Experiments with NbN-Based SIS Junction," to be published.

18. W. J. Skocopl, M. R. Beasley, and M. Tinkham, "Self-Heating Hotspots in Superconducting Thin-Film Microbridges," J. Appl. Phys., vol. 45, no. 9, pp. 4054-4066, Sep. 1977.

19. A. R. Kerr, S.-K. Pan, and M. J. Feldman, to be published.

20. J. R. Tucker, "Predicted Conversion Gain in Superconductor-Insulator-Superconductor Quasi-Particle Mixers," Appl. Phys. Lett., vol. 36, no. 6, pp. 477-479, March 1980.

21. M. J. Feldman, "Some Analytical and Intuitive Results in the Quantum Theory of Mixing," J. Appl. Phys., vol. 53, no. 1, pp. 584-592, Jan. 1982.

22. J. H. Greiner, et al., "Fabrication process for Josephson Integrated Circuit," IBM J. Res. Develop., vol. 24, no. 2, pp. 195-205, March 1980.

23. R. Holm, "Electric Contacts," New York: Springer-Verlag, pp. 15-16, 1967.

APPENDIX A: ANALYSIS OF MIXER MEASUREMENTS

We wish to analyze the RF performance, in particular, the differential resistance of the pumped dc I-V curve of these junctions. Tucker [20] and Feldman [21] have shown that within a certain range of the bias voltage V_o, pump voltage V_{LO} and local oscillator termination $G_{LO} + jB_{LO}$, the differential resistance of the dc I-V curve can be infinite, or even negative. In testing an SIS mixer, we always look for this effect first for the following reasons:

1) In the low IF limit, a negative output differential resistance implies that infinite conversion gain is available into an appropriately matched IF load. Thus the presence of the negative resistance indicates that the quality of the mixer is good, and it is capable being operated in the quantum regime.

2) As shown in Ref. [4], for a given V_o and V_{LO}, the source admittance plane of junction can be divided into two regions. In one region, the mixer output resistance is negative; in the other, it is positive. The boundary between these regions is the infinite output resistance line. Since the output resistance is directly related to the source admittance, analyzing the pumped dc differential resistance provides direct information about the range of available junction embedding admittances.

In order to compute the output resistance from theory it is necessary to know the available embedding admittance of the mixer mount very accurately. The type-D mixer mount used in this work has been carefully characterized by using a 40 x scale model. An equivalent circuit of the mixer mount, excluding losses, is shown in Fig. A-1. This equivalent circuit has been found in good agreement with the scale model measurements. In computing embedding impedances, loss in the suspended stripline and waveguides is taken into account. It is found that, except for a small forbidden region, the embedding admittance seen by the junction can be varied over almost the entire Smith chart by adjusting the two backshorts. Fig. A-2 shows a Smith chart plot of the available junction embedding admittance (C_J excluded) calculated from the equivalent circuit at 113.9 GHz. A detailed description of the characterization of mixer mount is given in chapter 4 of Ref. [4].

Adopting value quoted by Hypres for the specific capacitance of the junctions (30 $fF/\mu m^2$), the differential resistance of the pumped dc I-V curve at the first photon step below gap was calculated using Tucker's theory for the range of pump voltages used in our experiments. It was found that in a certain range of embedding admittances, the differential resistance can be negative. The results of a typical calculation are shown on the Smith chart plot of Fig. A-2.

Experimentally, however, as shown in Fig. 5(b), these junctions can only be tuned for positive and, at most, infinite output resistance. Since the embedding admittance of the junction is well understood, we conclude that the value of the specific capacitance of junction, C_s = 30 $fF/\mu m^2$, must be too low. The same calculation was carried out assuming C_s = 60 $fF/\mu m_2$, the value reported by Gurvitch *et al*. This result is also plotted in Fig. A-2 for comparison. In this case the pumped dc differential resistance of the junction is positive and, at most,

infinite which is in agreement with the experimental observations. We feel this strongly supports a value of 60 $fF/\mu m^2$ for the specific capacitance of these $Nb/Al\text{-}Al_2O_3/Nb$ junctions, rather than the 30 $fF/\mu m^2$ quoted by Hypres. The accuracy of this conclusion depends particularly on the correct mount losses being used in the simulation. However, it is difficult to account for the observed mixer performance using the lower specific capacitance without increasing the assumed mount losses to an unreasonable extent.

APPENDIX B: DESIGN AND ANALYSIS OF THE TUNING CIRCUIT

INTRODUCTION

Based on published results for SIS mixers, Feldman [1] concludes that a junction (or array of junctions) with an $\omega R_N C$ product of ~ 5 is desirable if performance close to that predicted by Tucker's three-frequency theory [1] is to be achieved. To match such a highly capacitive device to a real waveguide impedance requires a more complex circuit than normally used with Schottky diode mixers. If movable waveguide short-circuits are used as matching elements, it is often difficult to achieve broadband tuning -- broadband in the sense that the junction sees nearly equal impedances at the upper and lower sideband frequencies -- and it is even more difficult to arrange for both sideband embedding impedances to be in the range necessary for low conversion loss or some gain. For this reason many of the mixers we designed for fabrication by Hypres had an inductive tuning element integrated with the junction or array to tune out the junction capacitance.

In the ideal case, a lumped inductance connected across the junction would tune out the junction capacitance and allow an instantaneous RF (fractional) bandwidth of about $1/\omega R_N C$. (This approximation assumes the input conductance of the junction operating as a mixer is R_N, which is usually true within a factor of 2). The lumped tuning inductance needs a blocking capacitor if it is not to short-circuit the junction at DC and IF. In a practical mixer, additional fixed and adjustable tuning elements may be needed to couple efficiently between the waveguide and the junction over a reasonable tuning range. The instantaneous bandwidth is not then as wide as in the ideal case, but can be sufficient to allow the upper and lower sidebands to optimally matched.

A typical inductively-shunted two-junction array and its simplified equivalent circuit are shown in Fig. B-1. The array is shunted by a very short two-wire transmission line stub (loop) whose inductance is determined by the position of the shorting bar. Blocking capacitors are formed by anodizing the transmission line legs to form a layer of Nb_2O_5 (ε_r = 30) before depositing the Nb shorting bar. The inductance of the loop for various positions of the shorting bar was determined experimentally using a 500 x scale model in which the junction (or array) was represented by a chip-capacitor. Swept frequency measurements were made with the model SIS chip connected in series with a 50-ohm source and detector. A sharp dip in the detector output indicated the parallel resonance of the inductive shunt and the chip capacitor. (The sharpness of this resonance is a result of modelling the SIS junction by its capacitance only, corresponding to an infinite $\omega R_N C$). From measurements with a number of positions of the shorting bar a graph was plotted of loop inductance vs. position.

Tests of the first inductively-shunted Hypres junctions gave extremely disappointing results. In the ensuing period of diagnosis we made careful mixer measurements on the SIS arrays without inductive shunts, and concluded that the specific capacitance of the junctions was near 60 $fF/\mu m^2$, twice the original design value supplied by Hypres (these measurements are described in detail in Appendix A). Furthermore, we constructed 1000 x scale models of the 0.005" x 0.010" chips, in which the junctions were simulated by chip resistors and chip

capacitors in parallel. From measurements on these models we found that the equivalent circuit of Fig. B-1 was seriously over-simplified.

MEASUREMENTS ON A 1000 x SCALE MODEL OF THE SIS CHIP

A 1000 x scale model of the 0.005" x 0.010" SIS chip, including the bonding pads, was made on a printed circuit board. Fig. B-2(a) shows the details of the model. The bonding pads were connected at their ends to a ground plane below and parallel to the printed circuit board. The ground plane was far enough below the conductor pattern not to interfere with the behavior of the resonant circuit around the junction. A vector network analyzer was used to measure the impedance at the reference plane RP in Fig. B-2(a).

From the equivalent circuit of Fig. B-1(b) we expect the measured impedance to vary with frequency as shown in Fig. B-2(b). The impedance measured on the scale model, however, was substantially different from this. An extreme example is shown in Fig. B-2(c), in which a large impedance transformation is apparent between the junction and the measurement plane. The element values R_J, C_J, C_B, and l all seemed to influence the transformer ratio. Clearly the equivalent circuit of Fig. B-1 is inadequate. The primary cause of this was found to be the inductance between points A and B (Fig. B-2(a)) in series with the SIS junctions. Including this series inductance in the equivalent circuit gave good agreement with the experimental results, but it was also necessary to include the mutual inductance between the series inductance and the transmission line stub (loop) for the equivalent circuit to be useful for different stub lengths. The resulting equivalent circuit is shown in Fig. B-3(a), and an alternative form in Fig. B-3(b).

The importance of the mutual inductance in the behavior of this circuit can be demonstrated by changing its value in the above examples. This is accomplished by changing C_B and the loop length l to give the same resonant frequency as before. Reducing the loop length increases the mutual inductance between the conductors, thereby reducing the value of L_1 in Fig. B-3(b) and reducing the unwanted impedance transformation. Replacing C_B by a short circuit in the scale model gave the measured results shown in Fig. B-4.

Scale models were used to measure L_1 and L_2 (Fig. B-3(b)) as functions of loop length l for the three basic circuit patterns used for the Hypres mixers. These results, shown in Figs. B-5 to B-7, are for arrays of 2 (or 1), 4, and 10 junctions, respectively.

DISCUSSION

The strong effect of the series inductance of the SIS array has important implications for future broadband SIS mixer designs. This is true not only for mixers with the particular tuning circuits described here, but for any mixer in which the capacitance of an array of junctions is tuned out by an inductive element connected across the array. In the extreme case, when the operating frequency is close to the resonant frequency of the series inductance and junction capacitance (i.e., the self-resonant frequency of the array), the necessary tuning inductance is extremely small, and the junction impedance is transformed to a small value as in Fig. B-2(c). (Omitting the tuning inductance would result in the junction impedance being transformed to a very large value). For an

inductively shunted array to work satisfactorily, the operating frequency must be well below the self-resonant frequency of the array.

AN ALTERNATIVE APPROACH: THE INDUCTIVELY TUNED FOUR-TERMINAL JUNCTION

The self-resonant frequency in the above discussion is that of the part of the circuit between the points at which the tuning inductor is connected -- points A and B in Fig. B-2(a). If the inductance between A and B can be reduced the circuit will be usable at higher frequencies. This inductance can be effectively eliminated by using the circuit shown in Fig. B-8. Here, the SIS junction is made with four leads, two for input and output, and two for the tuning inductor. It is thus possible to connect the inductor directly to the junction terminals.

Measurements on a 1000 x scale model of such an inductively tuned four-lead SIS junction of Fig. B-9(a) are shown in Fig. B-9(b). It is immediately apparent that we now have another impedance transformation between the junction and the external circuit, albeit a much smaller one than before. The cause is now the mutual inductance between the tuning loop and the leads to the external circuit. (This was verified by modifying the model to allow the tuning loop to be rotated about its axis so its plane was perpendicular to that of the rest of the circuit, thereby eliminating the mutual inductance).

The equivalent circuit of the inductively tuned four-lead junction is shown in Fig. B-9(c). Circuit analysis indicates that the impedance transformation ratio is given by

$$\frac{R}{R_J} = R_J \times \left[1 + \frac{M}{L_2}\right]^2$$

Measurements on the scale model for different stub lengths are summarized in Fig. B-10. For the particular resistor and capacitor used to simulate the junction in this model, $\omega R_J C$ is 5 at 115 MHz (corresponding to 115 GHz for the original circuit).

It is possible to connect several of these inductively tuned four-terminal junctions in series on a 0.005" x 0.010" chip. Fig. B-11(a) shows a model with 4 such junctions in series. The measured impedance of this array is shown in Fig. B-11(b). There is no evidence of undesirable coupling, either inductive or capacitive, between the separate circuits; however, we cannot rule out such effects for other combinations of R_J, C, and frequency.

APPENDIX C: THERMAL ANALYSIS

In this appendix, we give a very approximate thermal analysis of an SIS chip mounted in a mixer block and cooled to 4.2 K in a vacuum.

As shown in Fig. 1, the SIS chip is cold-welded to the indium pads on a fused quartz substrate which is heat sunk at one end to the mixer block and at the other end to the center pin of the SMA connector. Since the thermal conduction of the gold stripline circuit patterns on the substrate is very good, we can assume that the temperature at the bonding pads is 4.2 K. In the SIS chip, heat is generated by ordinary joule heating. If the junction is biased at the gap voltage (~ 2.8 mV) with a dc bias current around 1/2 I_c (~ 200 μA in sample Hypres-WN430-C5-M7-DII0 which is shown in Fig. 8(b)), the power dissipated in each junction is ~ 0.6 μW. This heat is removed from each junction, as shown in Fig. C-1, in two ways: by thermal conduction within the niobium thin film to the bonding pads, and by conduction across the niobium/fused quartz boundary and through the fused quartz of the chip to the bonding pads. Since the size of the junctions (~ 2μm in radius) is relatively small compared to the size of the chip (254 μm long x 127 μm wide x 127 μm thick), the approximate spreading thermal resistance of the fused quartz chip can be estimated by treating junction as a small point heat source embedded in a semi-infinite conducting medium with uniform thermal conductivity σ. The thermal resistance of the chip is then [23]:

$$R_{chip} = 1 \; / \; 4\sigma a$$

where a is the radius of the junction. Taking σ = 1 mW/cm·K for fused quartz, we find that R_{chip} is ~ 1.2 K/μW.

The thermal resistance of the niobium thin film, R_{Nb}, can be calculated by using the formula:

$$R_{Nb} = 1 \; / \; K(T) \cdot W \cdot D$$

where l, W and D are the film length, width, and thickness, respectively, and K(T) is the temperature dependent thermal conductivity of the niobium film. Above the critical temperature (9.3 K for Nb), K(T) can be estimated from electrical conductivity of the film by using Wiedemann-Franz law:

$$K(T) = (\pi^2/3)(k_B/e)^2 \cdot T \cdot \sigma(T).$$

Using σ = 1.59 x 10^5 $\mu\Omega^{-1}cm^{-1}$ at 9.3 K [22], we calculate K(T=9.3K) to be ~ 3.6 mW/cmK. Since the thermal conductivity of a metal is reduced if it goes into the superconducting state, this estimate provides an upper limit on K(T=4.2K). For a niobium conductor 14 μm long x 7 μm wide x 2000 A thick, we conclude that the thermal resistance > 2.8 K/μW.

Calculation of the actual temperature rise in our array is complicated by the fact that we have ten junctions in series and there is no published value for the thermal interface resistance between Nb and fused quartz**, but it is clear that a temperature rise of the order of 1 K is possible.

From the B.C.S. theory, in the neighborhood of T_c, the energy gap may be expressed by the following approximate formula [15]:

$$\Delta \sim 3.2\, k_B T_c\, (1 - T/T_c)^{1/2}$$

thus increasing the junction temperature from 4.2 K to 5.2 K will reduce the gap voltage by about 10% which is roughly the reduction observed on Fig. 8(b).

** For Sn/glass or Sn/sapphire, the interface thermal resistance is of the order of 50 $\mu m^2 K/\mu W$ [18].

APPENDIX D: PERFORMANCE ON THE 12-m TELESCOPE, MARCH 1987

The performance of these mixers in the receiver on the 12-m Kitt Peak radio telescope is shown in Fig. D-1. The receiver has two channels, one for each linear polarization, identified by numerals 1 and 2 in Fig. D-1. The receiver is normally operated in the single sideband mode with the tuning adjusted to reject the image sideband by at least 20 dB. Characters U and L in Fig. D-1 indicate operation in the upper and lower sidebands.

The increase in receiver noise temperature near 110 GHz is thought to be a result of having insufficient LO power in this range. Measurements in the laboratory using the same mixer design have generally shown smooth variation of T_R with frequency over the full range.

It will be noticed that the values of T_R given in Fig. D-1 for the telescope receiver are somewhat higher than those quoted elsewhere in this report which were measured at the room-temperature feed horn of our laboratory test dewar. The reason for the difference is primarily the additional room temperature input loss of the quasi-optical components on the telescope receiver. Fig. D-2 shows a noise analysis of the telescope receiver.

TABLE I. Effective IF Noise Temperature with Different IF Bands

IF Center Frequency & Bandwidth	Effective IF Noise Temperature
1400/25 MHz	13.6 K
1390/50 MHz	15.9 K
1450/700 MHz	21.2 K

TABLE II. Typical Mixer and Receiver Properties of the Nb/Al-Al_2O_3/Nb Junctions of Hypres Wafer WN-430 (j_c = 1400 A/cm^2) with $f_{sig.}$ = 115.3 GHz, f_{LO} = 113.9 GHz and f_{IF} = 1.4 GHz

Sample	# of Jns. in Array	Junction Size (μm)^2	R_{Array} (Ohm)	ωRC	Sideband Tuning	Mixer		Receiver Noise* Temp.	P_{LO} (μW)	Bath Temp. (K)
						L_C (dB)	T_M (K)			
Hypres-WN430 -C5-M7-DII0	10	3.75 x 3.75	57	4.6	SSB DSB SSB	4.63 1.86	16 4	81.7 49.5 95.6	2 0.5	2.5 2.5 4.2
Hypres-WN430 -C5-K11-DIII4	4	2.5 x 2.5	60	6.3	SSB DSB SSB	4.96 5.41	20.5 20.5	88.1 67.1 97	0.5 0.5	2.5 2.5 4.2
Hypres-WN430 -C5-R6-DII5	4	2.5 x 2.5	57	6.3	SSB DSB SSB DSB	4.94 2.99 5.17 3.54	19 11.5 23 12	89.3 64.2 95.6 68.5	0.65 0.1 0.36 0.14	2.5 2.5 4.2 4.2
Hypres-WN430 -D5-K5-DIII1	4	3 x 3	44	6.2	SSB DSB	5.79	29	110 79		4.2 4.2
Hypres-WN430 -C7-F6-JJ	10	2.25 x 2.25	200	7.3	DSB DSB	4.3	15	77.8 99.8	0.21 0.21	2.5 4.2

*As measured at the room temperature feed-horn. No corrections have been made for input losses.

TABLE III. Receiver Noise Temperature Using Hypres WN430-C5-R6-DII5 with Different IF Bandwidths

IF Bandwith	SSB T_R	DSB T_R
1400/25 MHz	105 K	70.2 K
1390/50 MHz	114.5 K	74.3 K
1450/700 MHz	144 K	93.4 K

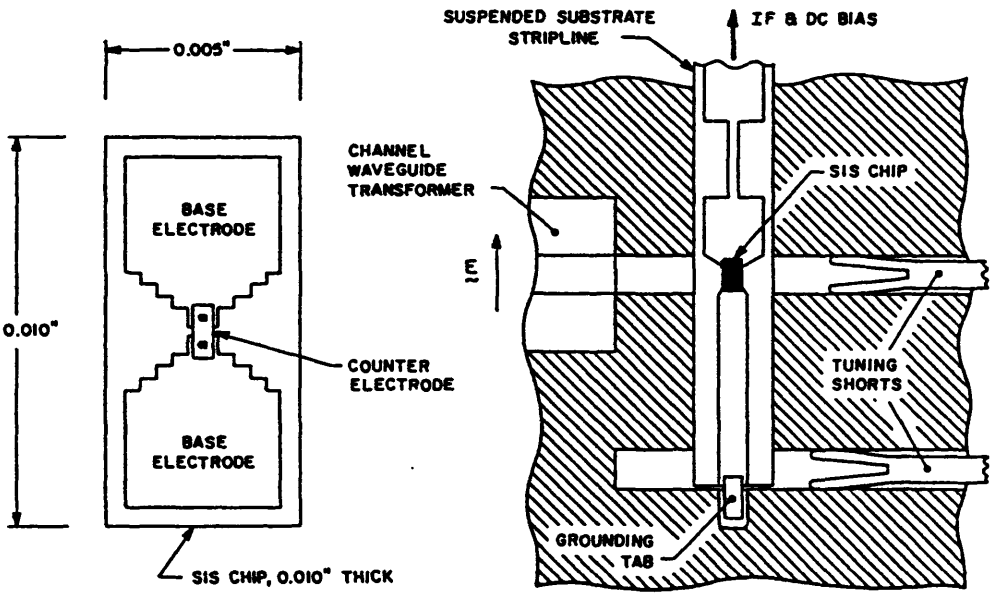

(a)

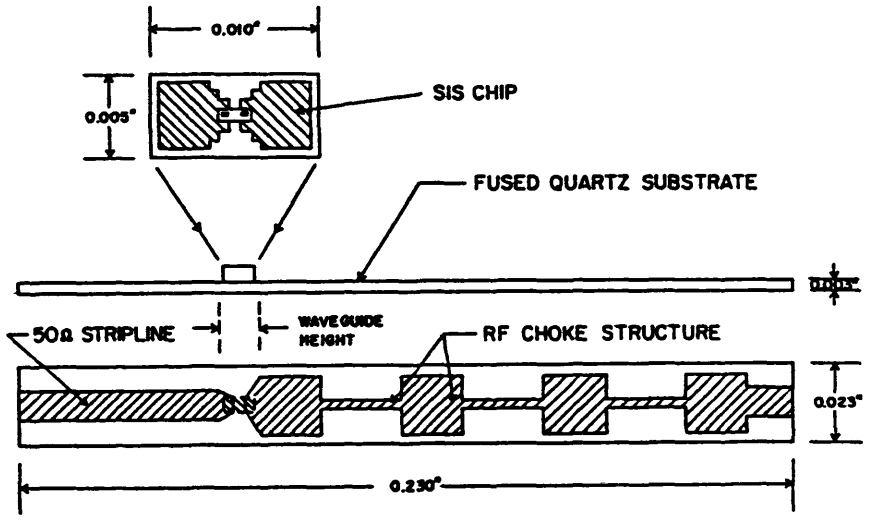

(b)

Fig. 1. a) Diagram of the type-D mixer mount.
b) Top and side views of the SIS chip and quartz substrate. The SIS chip is mounted on the substrate by cold welding with indium.

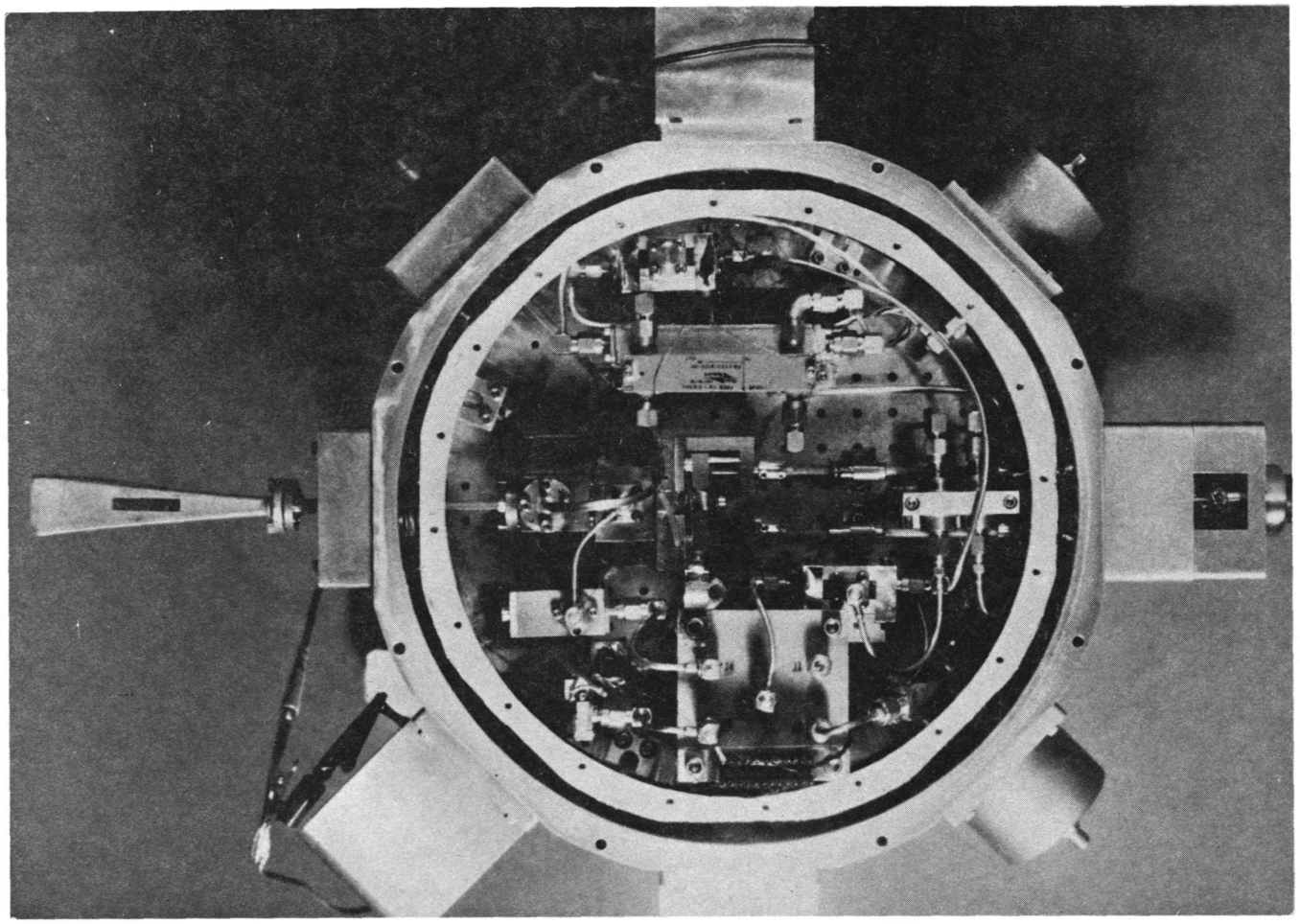

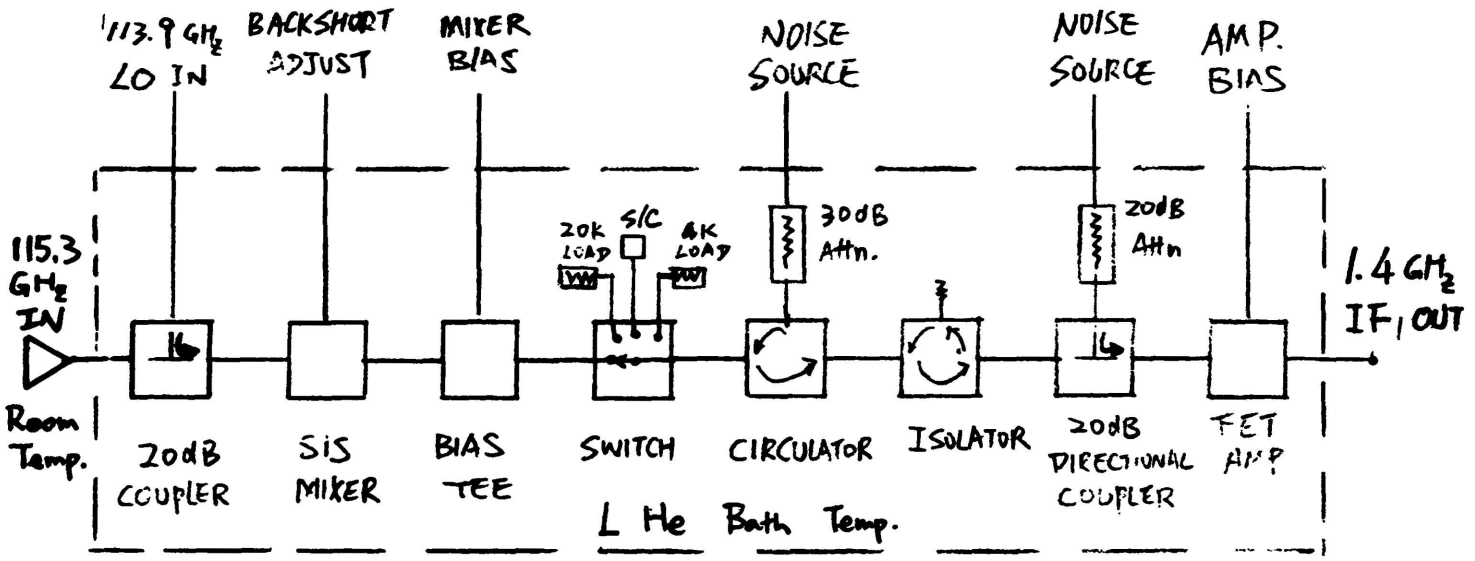

Fig. 2. Photograph and block diagram of the test receiver.

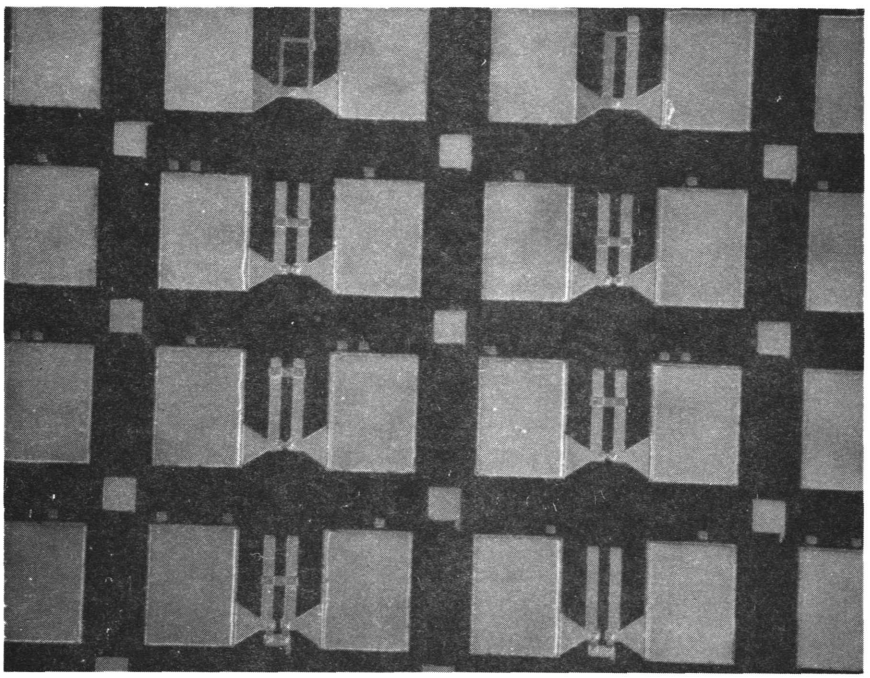

Fig. 3. Picture of part of a Nb/Al-Al_2O_3/Nb junction wafer. Each 3.2 mm square cell contains 220 mixer chips, each 127 μm x 254 μm. There are 96 different chip designs, with different numbers of junctions, junction sizes, and tuning circuits.

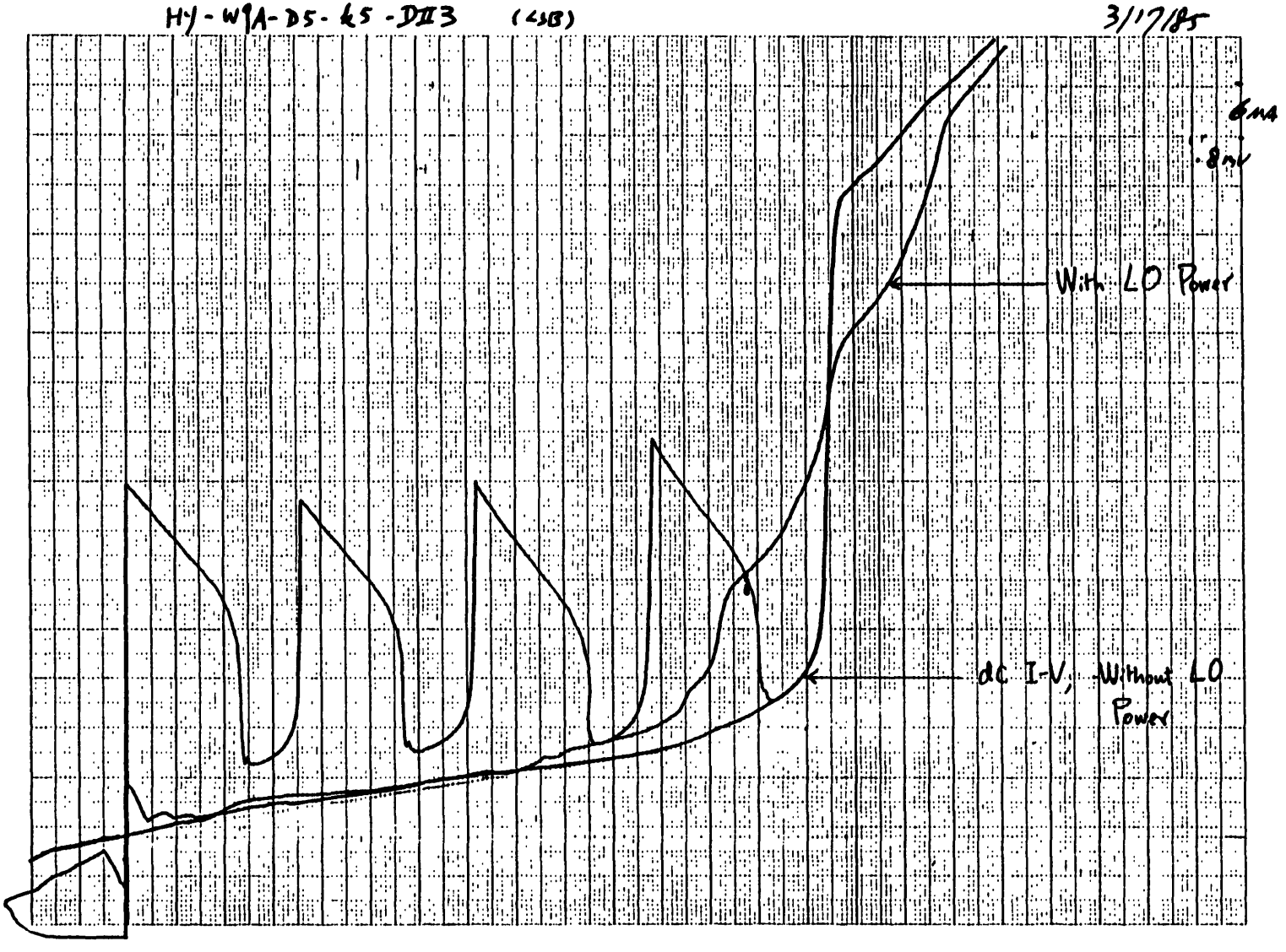

Fig. 4. 4.2 K I-V characteristic of a four-junction array from wafer W9A (J_C - 850 A/cm^2, V_m(2mV) - 26 mV).

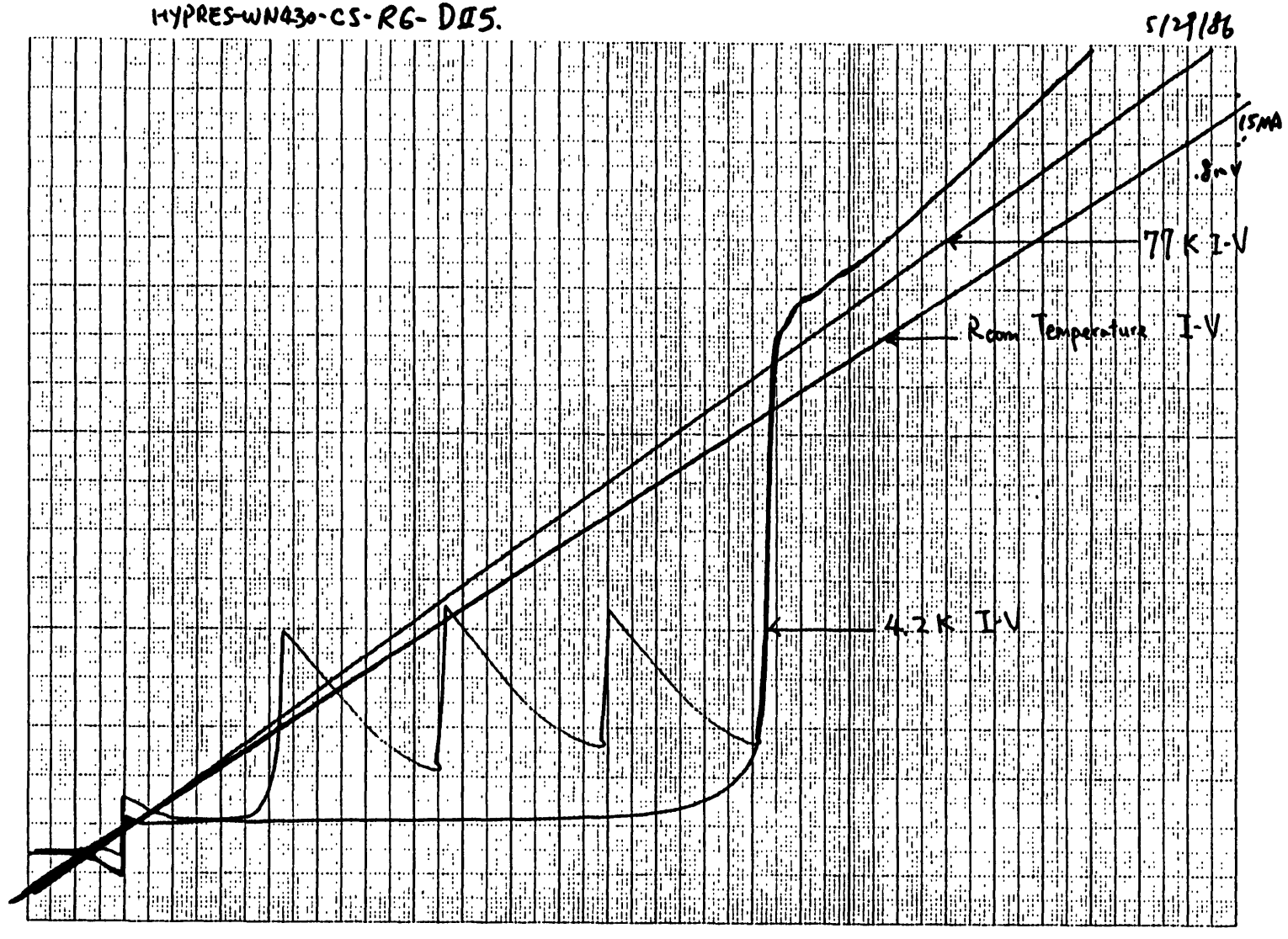

Fig. 5(a). 4.2 K I-V characteristic of a four-junction array from wafer WN430 (J_C ~ 1,400 A/cm^2, V_m(2mV) ~ 40 mV). Note that the room temperature junction resistance is higher than the tunneling resistance. Also, I(2Δ/e, T = 4.2 K) is higher than I(2Δ/e, T = room temperature).

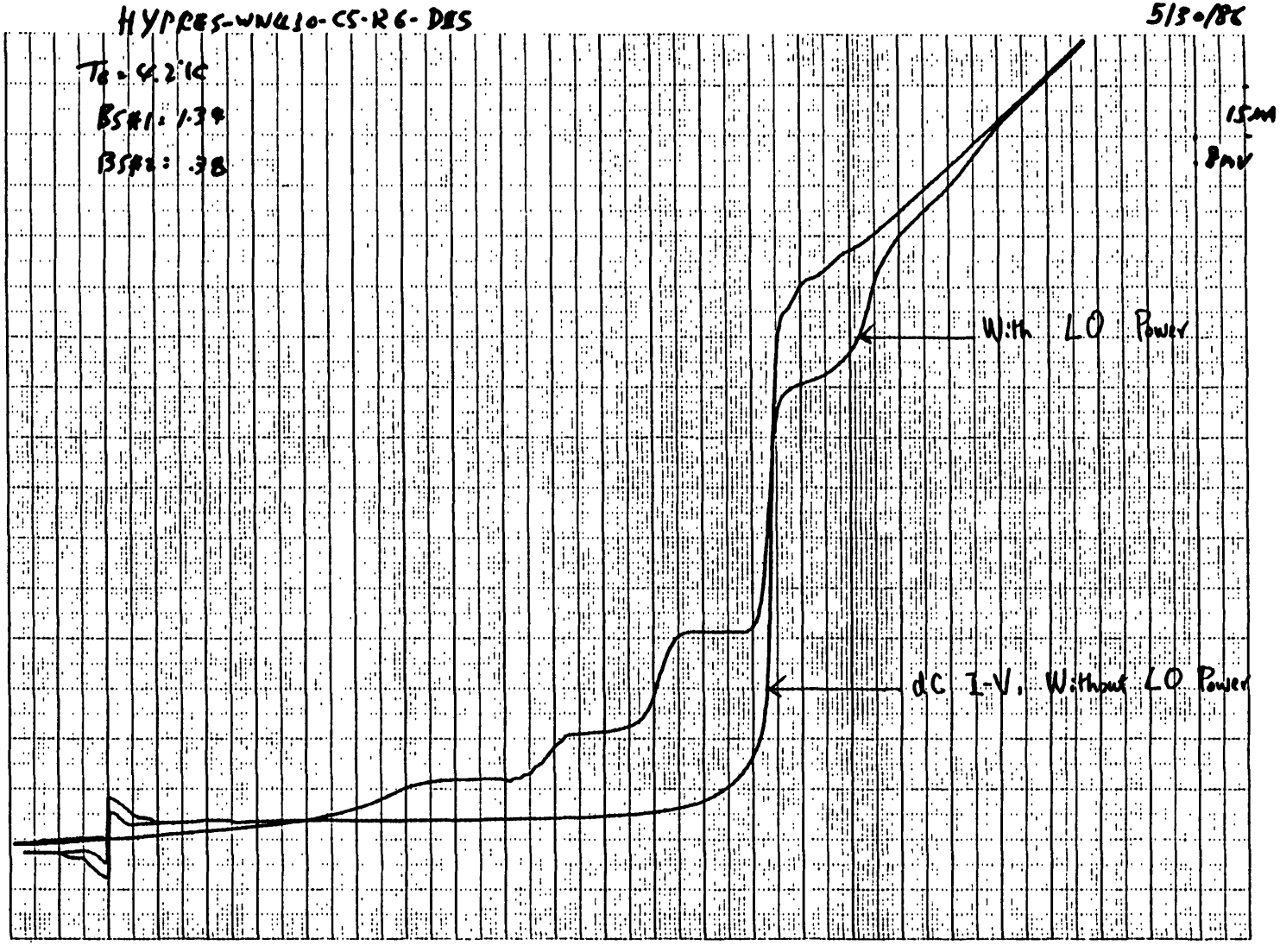

Fig. 5(b). Pumped dc I-V curve shows an infinite differential resistance at the first photon step below gap.

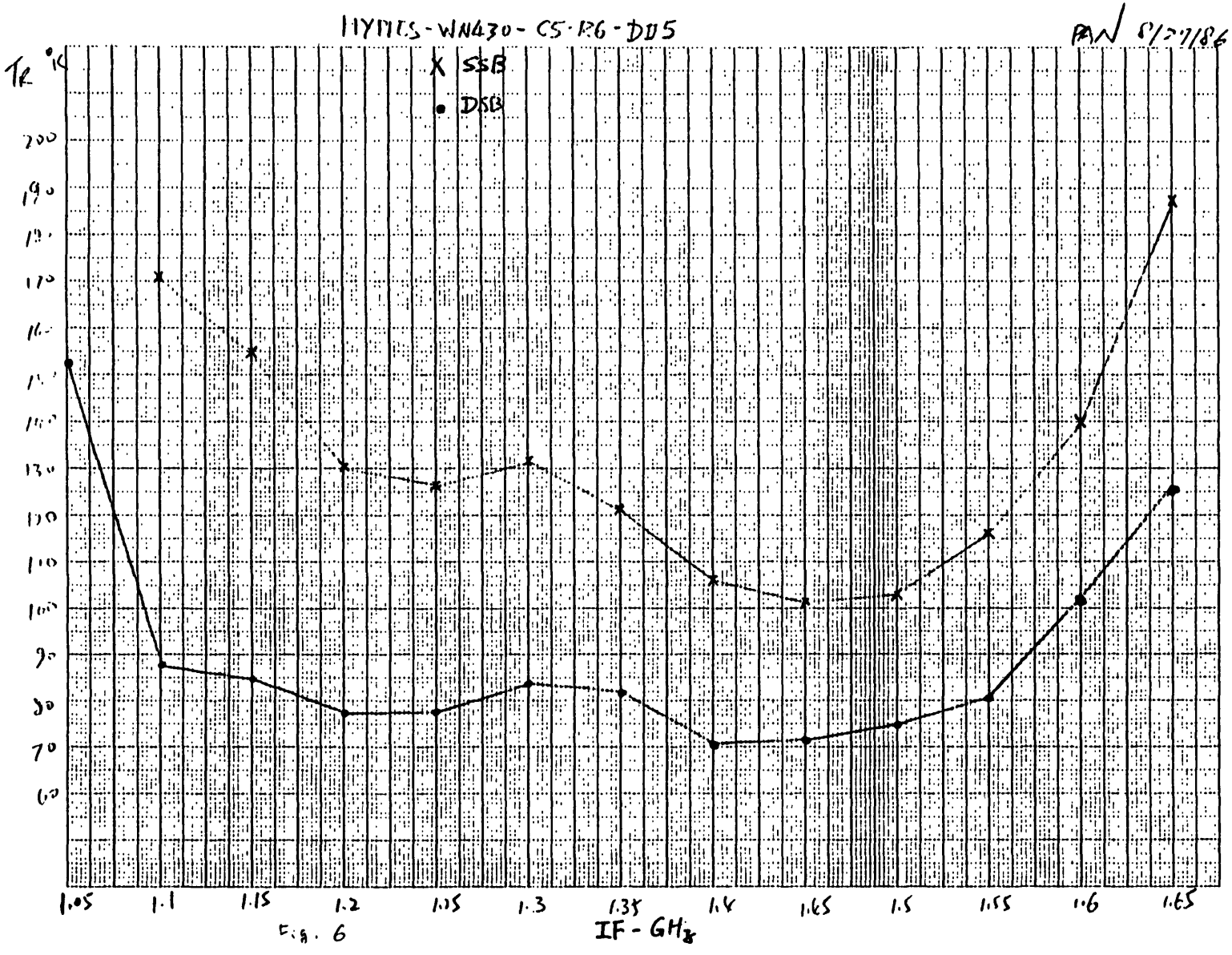

Fig. 6. Receiver's instantaneous bandwidth. Data obtained with fixed f_{LO}, P_{LO}, V_{dc} and backshort setting.

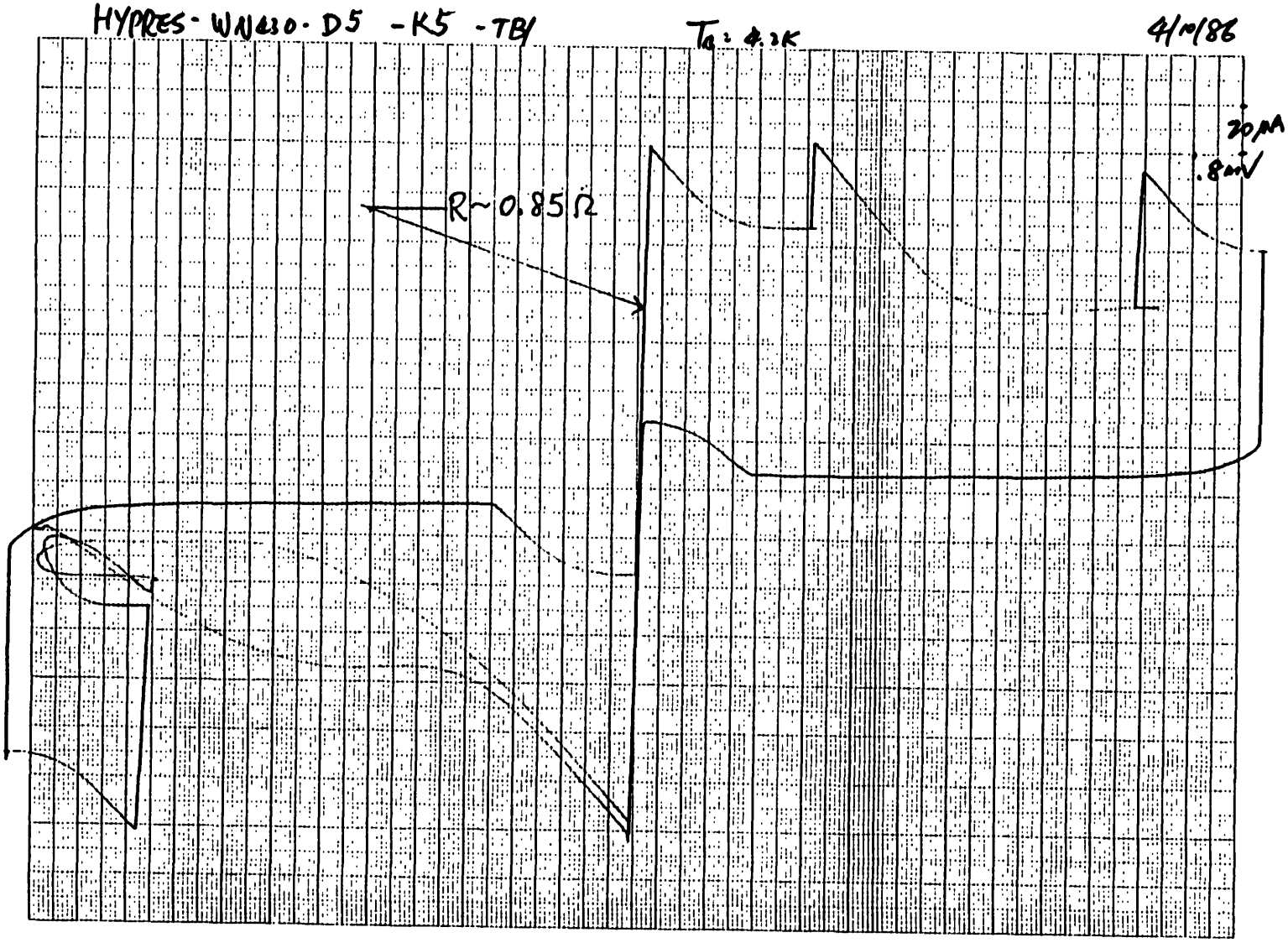

Fig. 7. Superconducting portion of the I-V characteristic of array Hypres-WN430-D5-K5-DIII1. The slope of the dc Josephson current corresponds to a series resistance of 0.85 ohm.

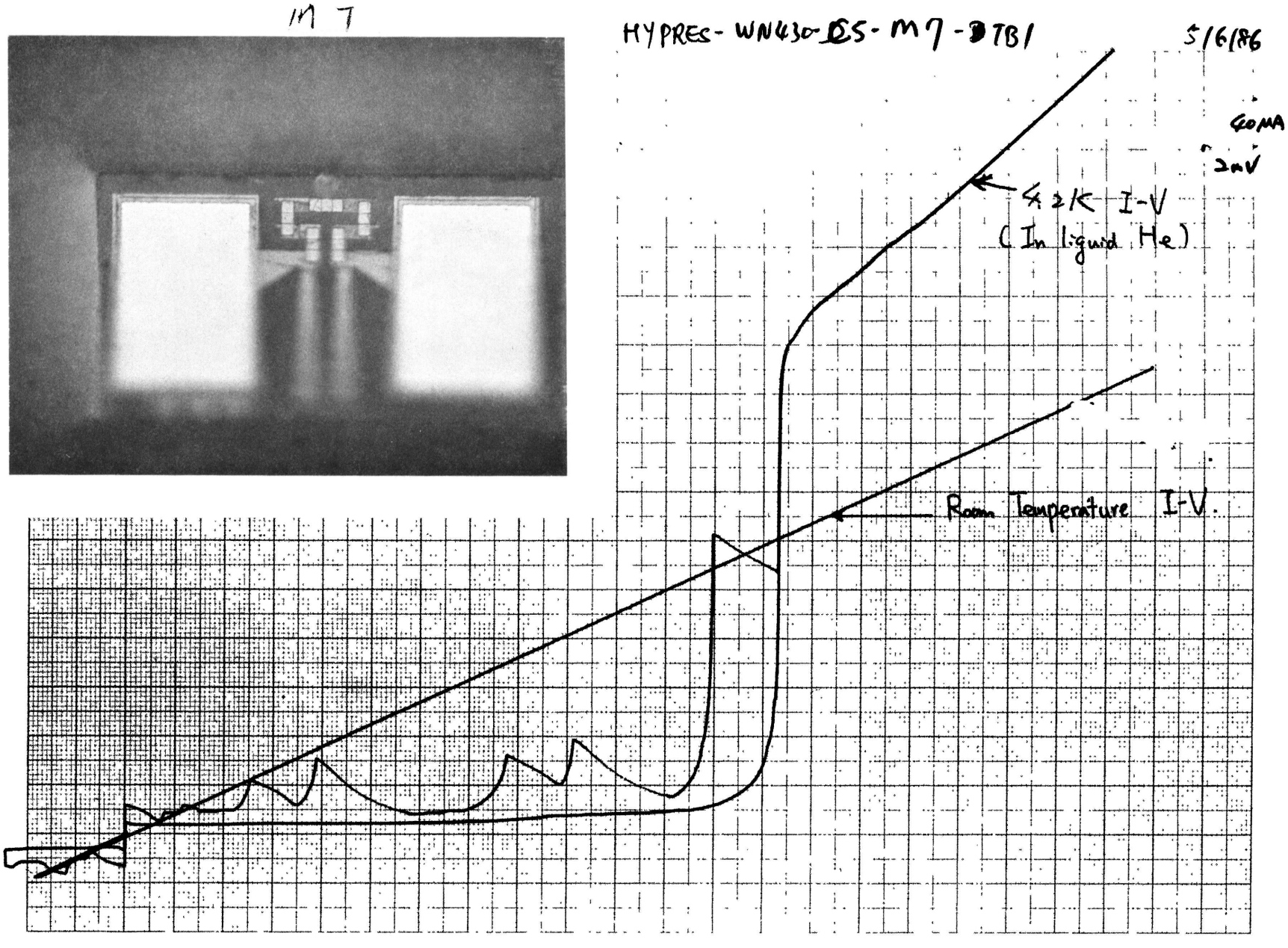

Fig. 8(a). I-V curve of sample Hypres-WN430-C5-M7-DII0 (J_C ~ 1,400 A/cm^2) when it is immersed in liquid helium. No heating effect is observed.

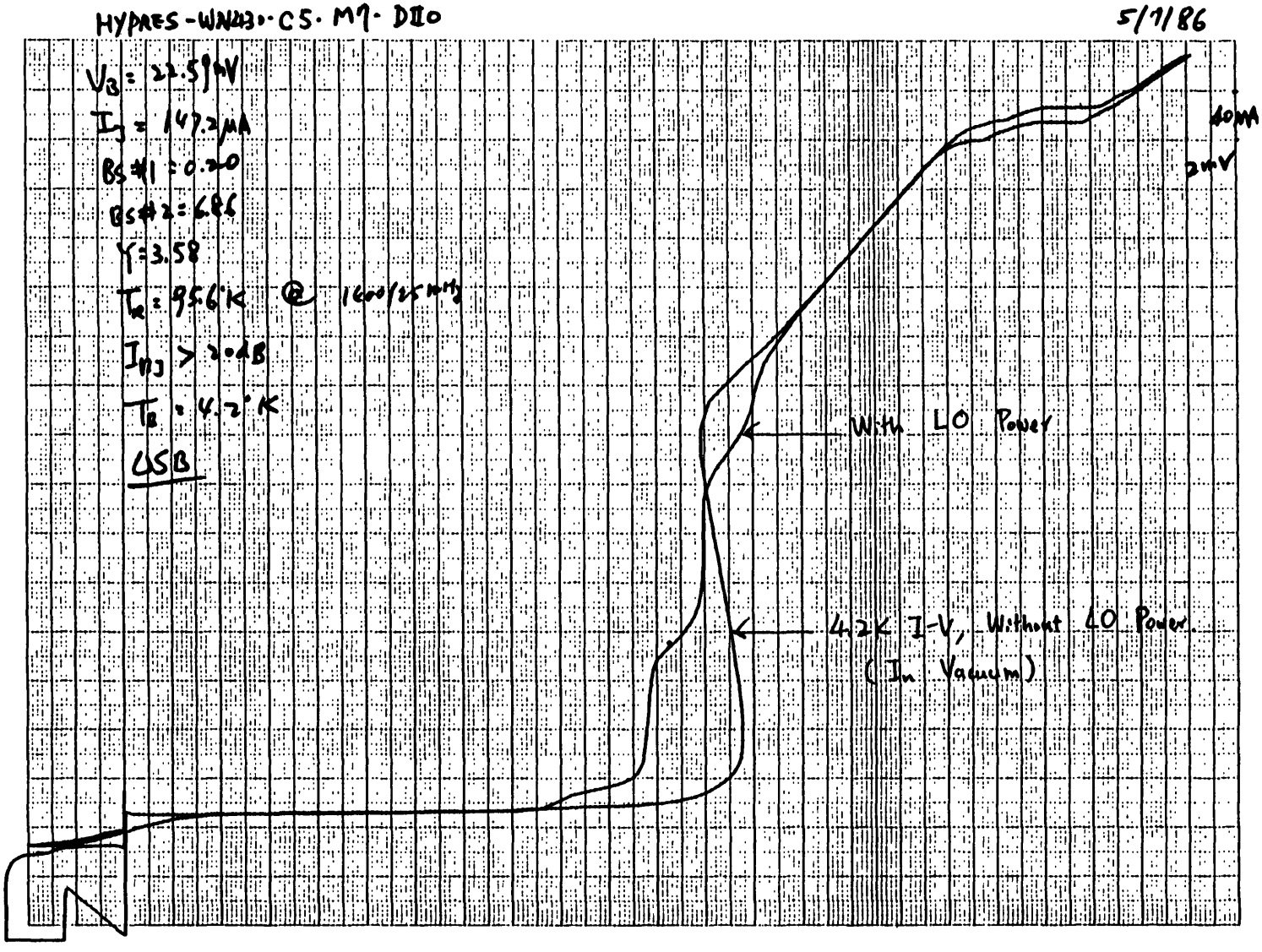

Fig. 8(b). 4.2 K I-V curve of the same sample as in Fig. 8(a), in vacuum. Heating effects are clearly seen.

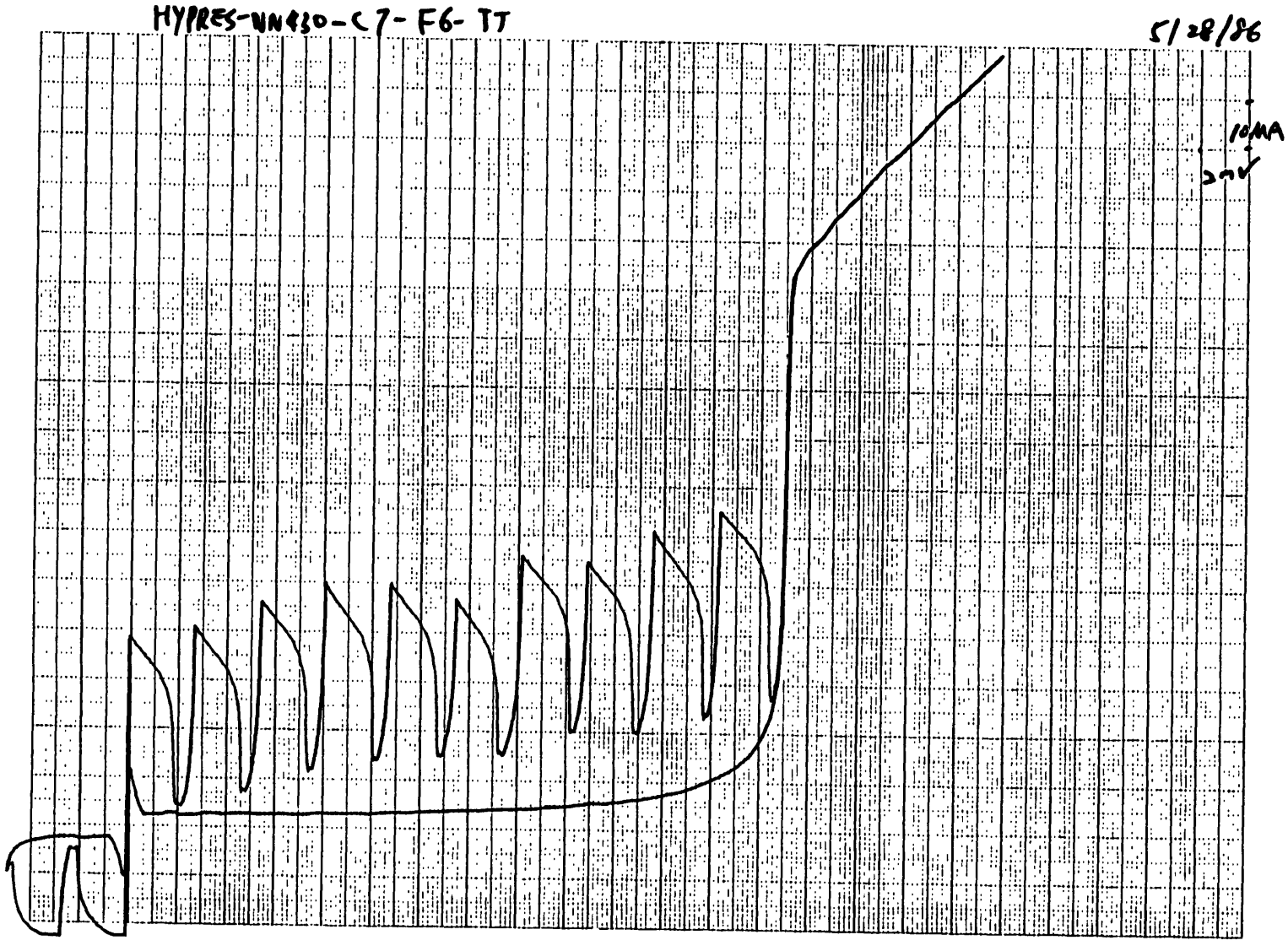

Fig. 9. I-V characteristic of a ten-junction array designed for 230 Gliz. The (nominal) junction size is 2.25 μm x 2.25 μm.

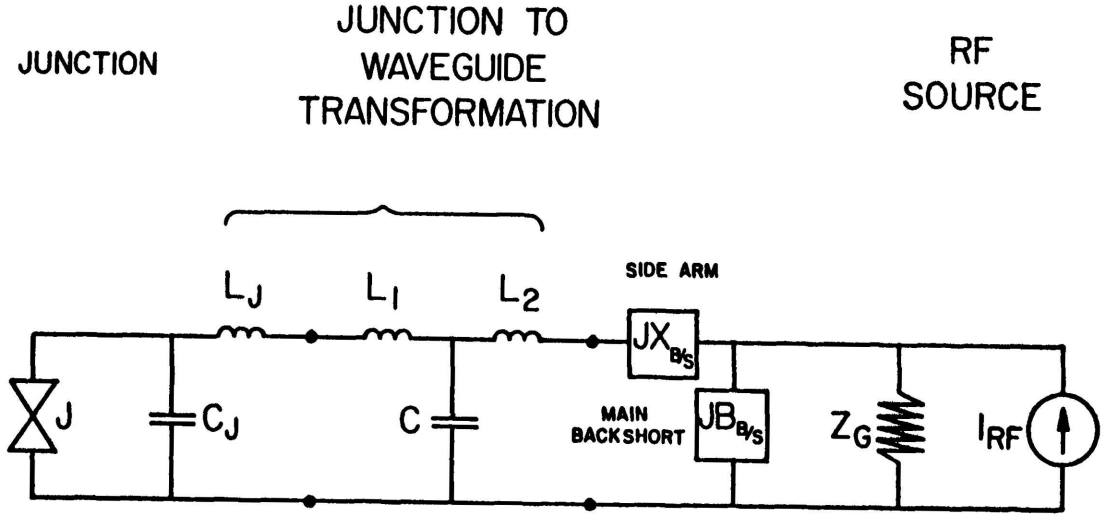

MICROWAVE EQUIVALENT CIRCUIT OF THE MIXER MOUNT

Fig. A-1. Microwave equivalent circuit of the mixer mount.

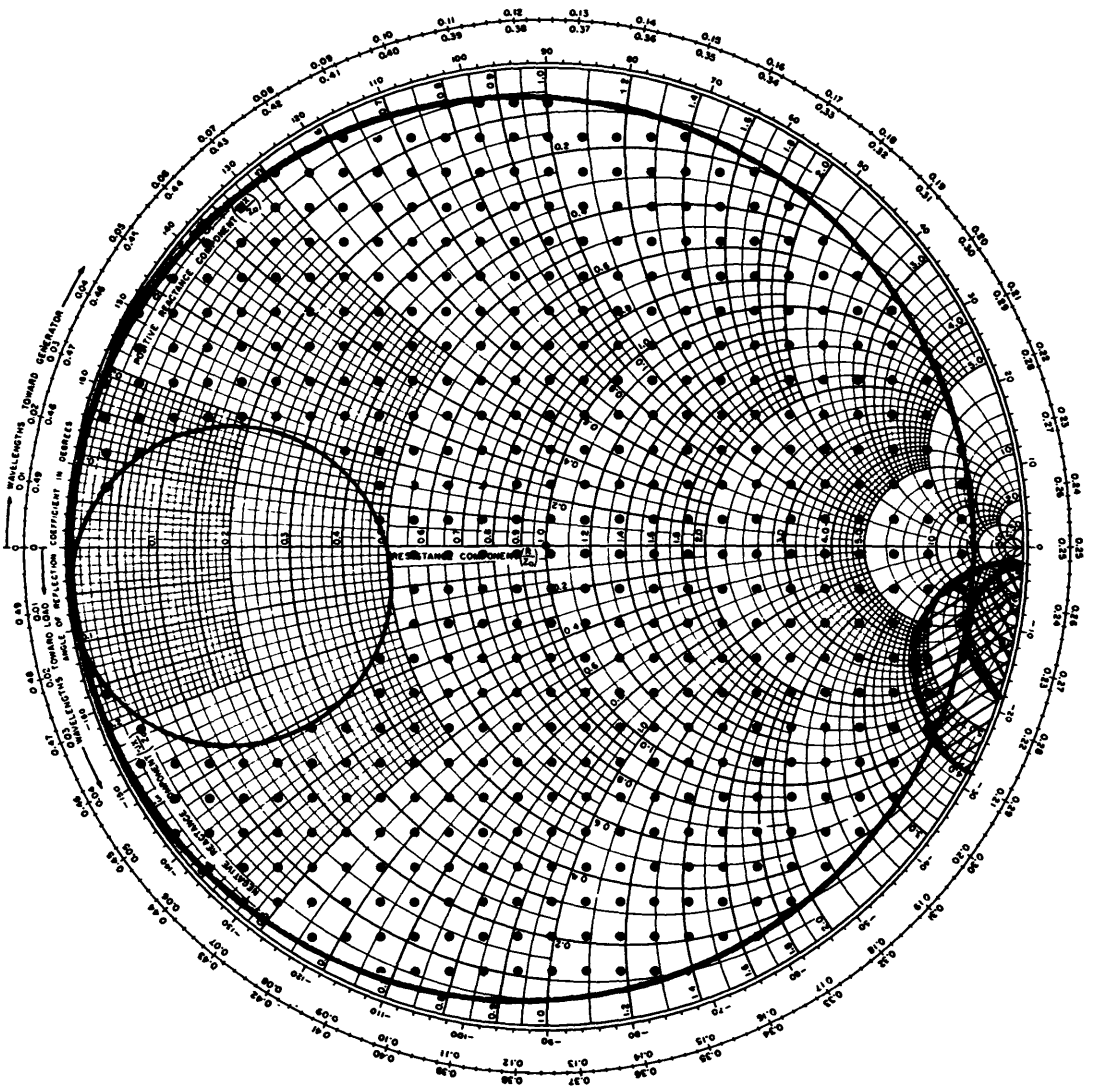

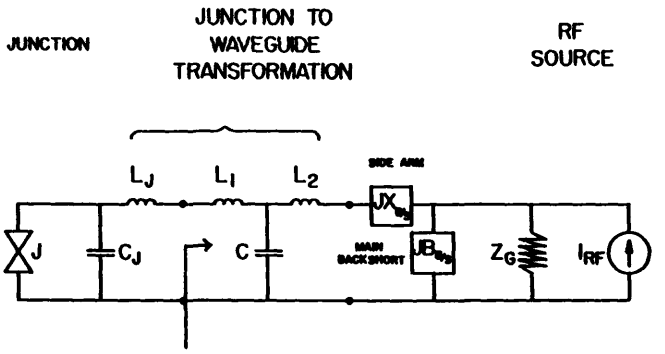

Fig. A-2. [: :] indicates the available embedding admittance region of the mixer mount calculated from the equivalent circuit shown in Fig. A-1. The reference plane is indicated by the arrow. Also shown is the calculated Y_{LO} range (referred to the same reference plane) which yields negative pumped dc differential resistance at the first photon step for the four-junction array Hypres-WN430-D5-K5-DIII1 assuming C_s = 30 fF/μm^2 (▨) and C_s = 60 fF/μm^2 (▩). In this calculation, V_o = 9.98 mV and $\alpha = e V_{LO}/\hbar\omega$ = 1.4 were used.

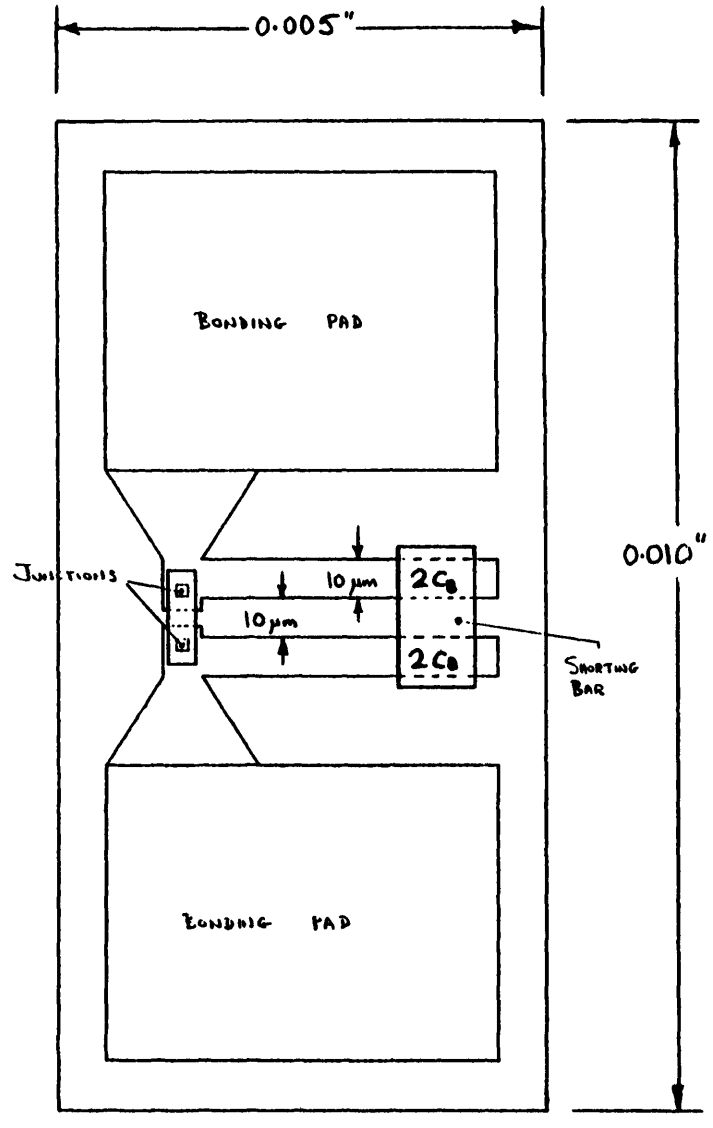

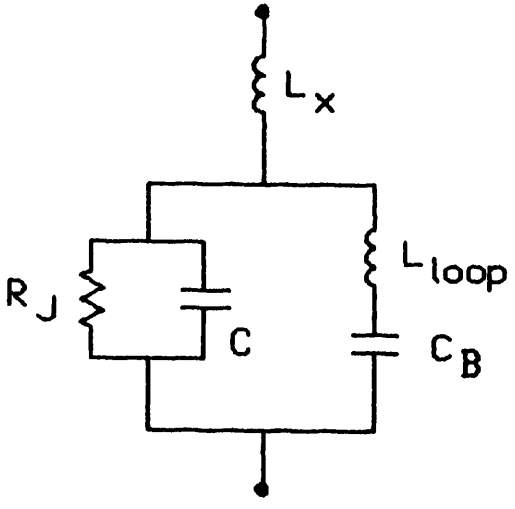

Fig. B-1(a) A typical two-junction array with an inductive tuning loop and blocking capacitors (total C_B).

Fig. B-1(b) Simple equivalent circuit for (a). The SIS array is represented by R_J and C. C includes the junction capacitance and the overlap capacitance between the upper and lower electrodes.

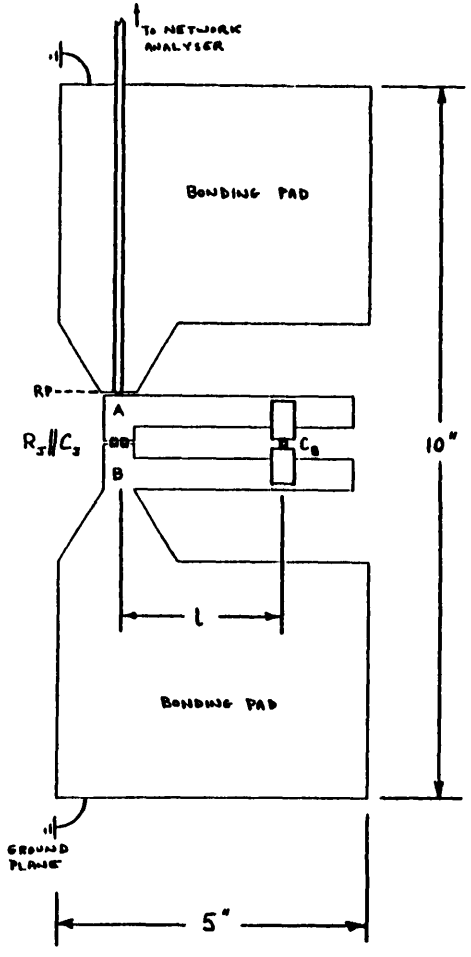

(a)

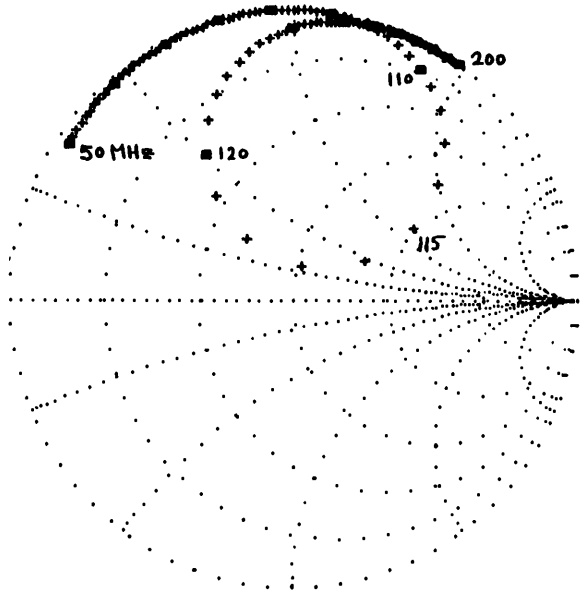

(b)

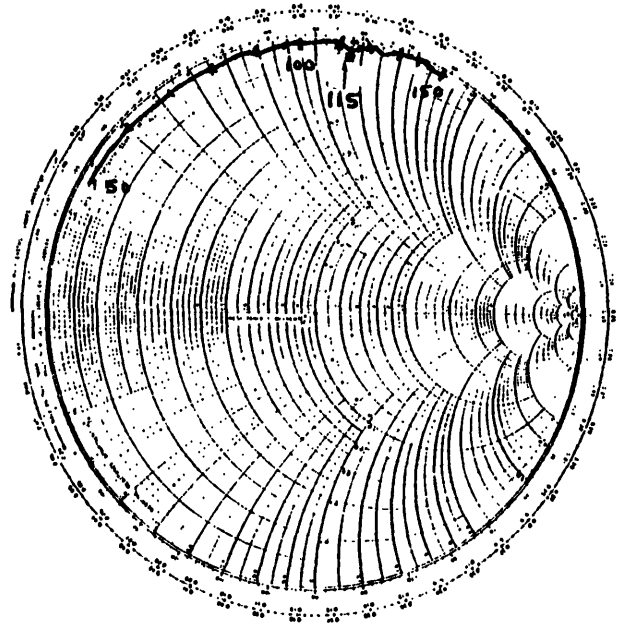

$R_J = 97\ \Omega$
$C_J = 161$ pF
$C_B = 98$ pF

$l = 36$ mm

(c)

Fig. B-2(a) 1000 x scale model of the SIS chip.

Fig. B-2(b) Expected impedance vs. frequency based on the equivalent circuit of Fig. B-1(b). (Smith chart normalized to 50 Ω).

Fig. B-2(c) Measured impedance vs. frequency, from which it is clear that a substantial impedance transformation is occuring.

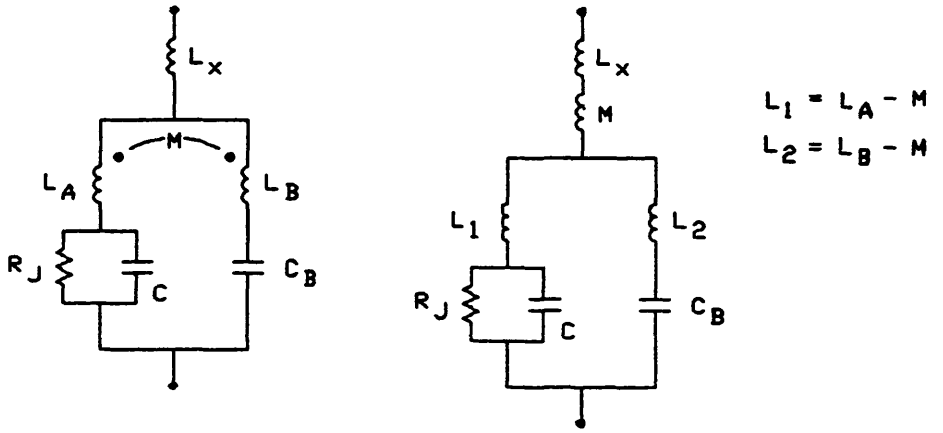

Fig. B-3(a) The improved equivalent circuit of the inductively tuned array ofFig. B-1(a).

Fig. B-3(b) Alternative form of (a).

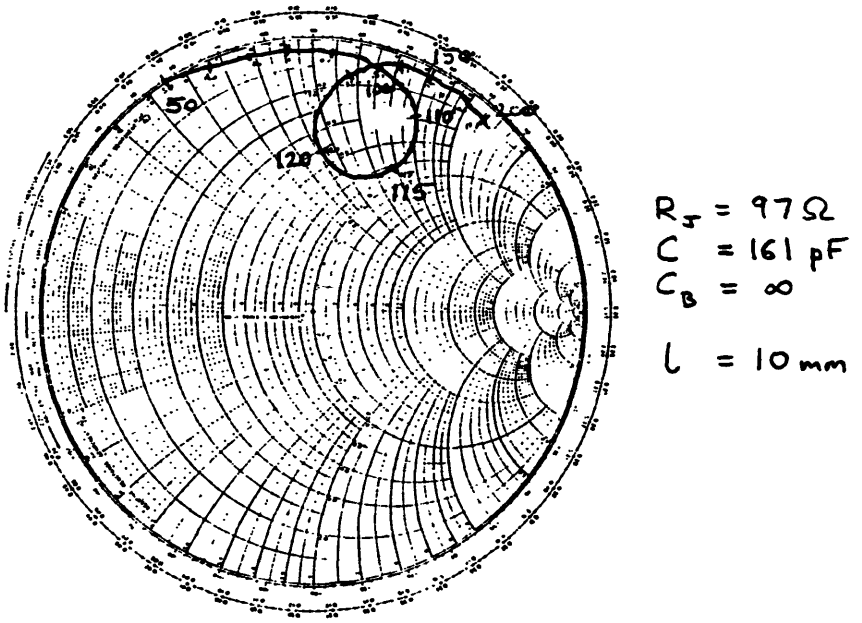

Fig. B-4 Measured impedance vs. frequency for the same circuit as in Fig. B-2(c), but with $C_B = \infty$ and length l reduced from 36 mm to 10 mm to give the same resonant frequency.

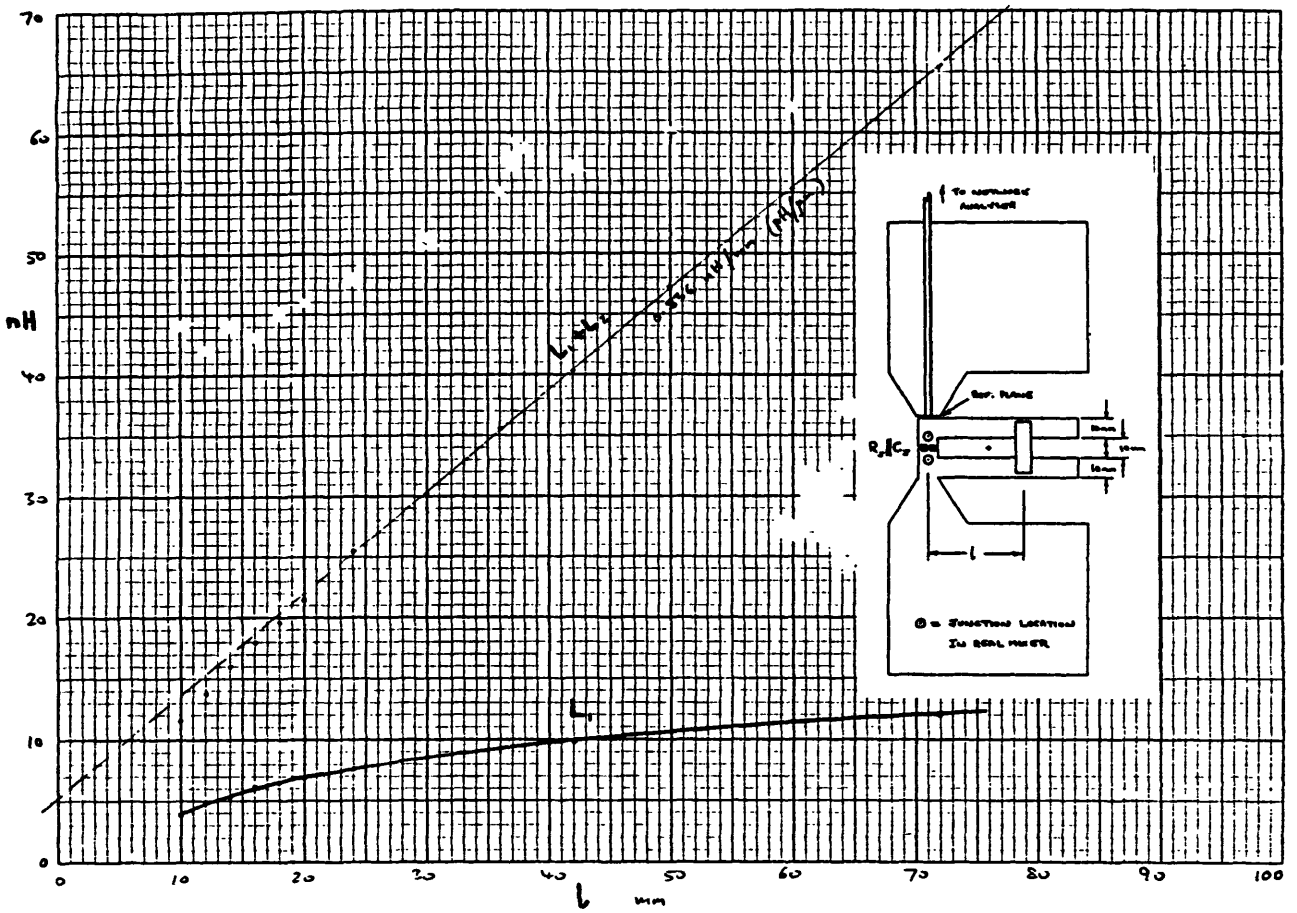

Fig. B-5 Values of L_1 and $L_1 + L_2$ as functions of loop length l, for the 1000 x scale model of a two-junction array.

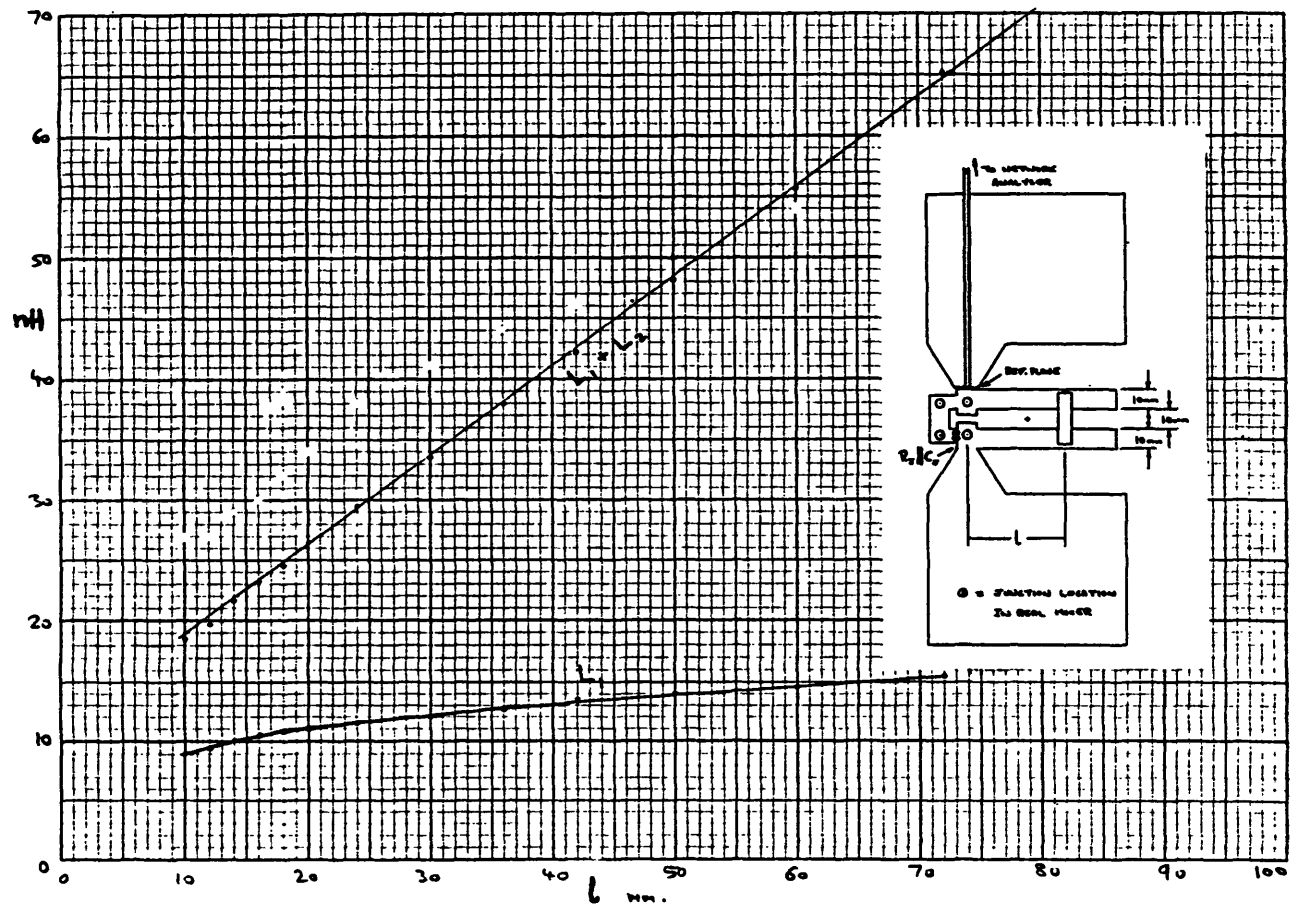

Fig. B-6 Values of L_1 and $L_1 + L_2$ as functions of loop length l, for the 1000 x scale model of a four-junction array.

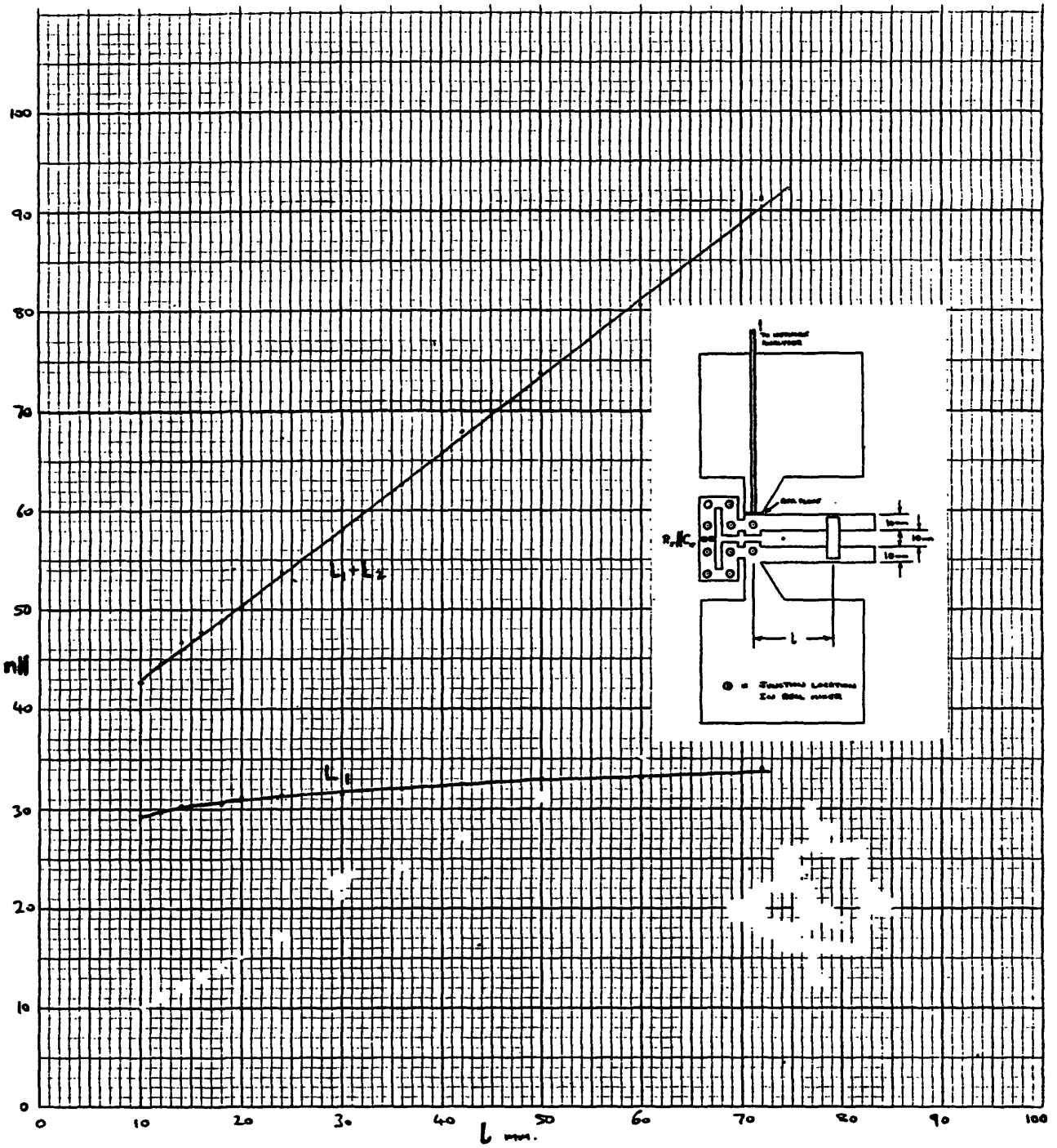

Fig. B-7 Values of L_1 and $L_1 + L_2$ as functions of loop length l, for the 1000 x scale model of a ten-junction array.

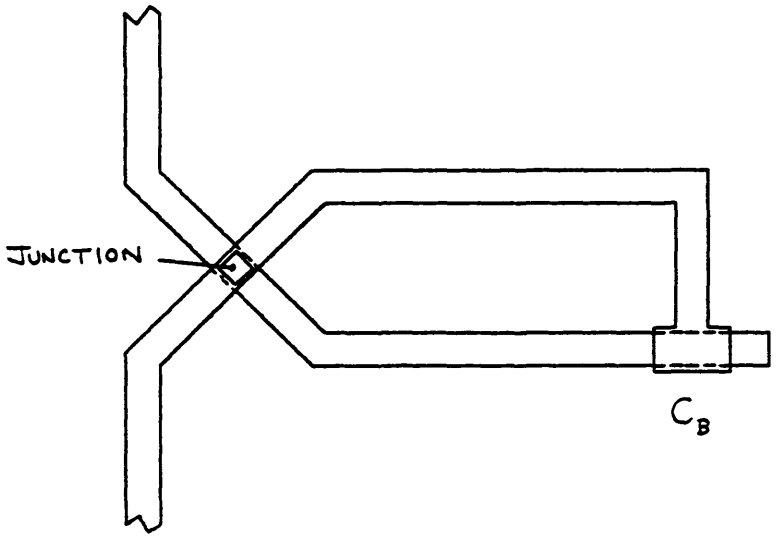

Fig. B-8 The inductively tuned four-terminal SIS junction. The current in the inductor does not flow in any part of the leads to the external circuit.

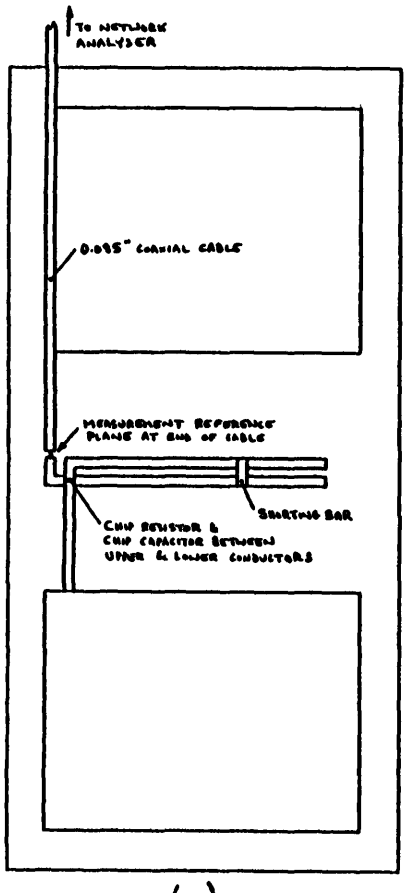

(a)

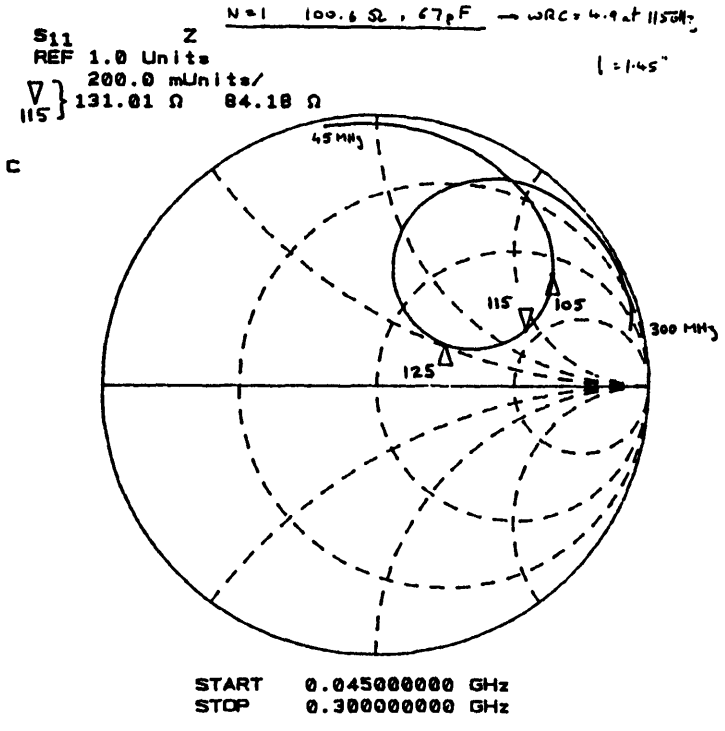

(b)

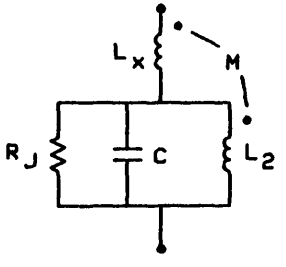

(c)

Fig. B-9(a) 1000 x scale model of an inductively tuned four-terminal SIS junction.

Fig. B-9(b) Measured impedance vs. frequency for the circuit of (a), from which it is clear that a small impedance transformation is occuring, but now in the opposite sense to that for the inductively tuned arrays of Fig. B-2(a).

Fig. B-9(c) Equivalent circuit of the inductively tuned four-terminal SIS junction.

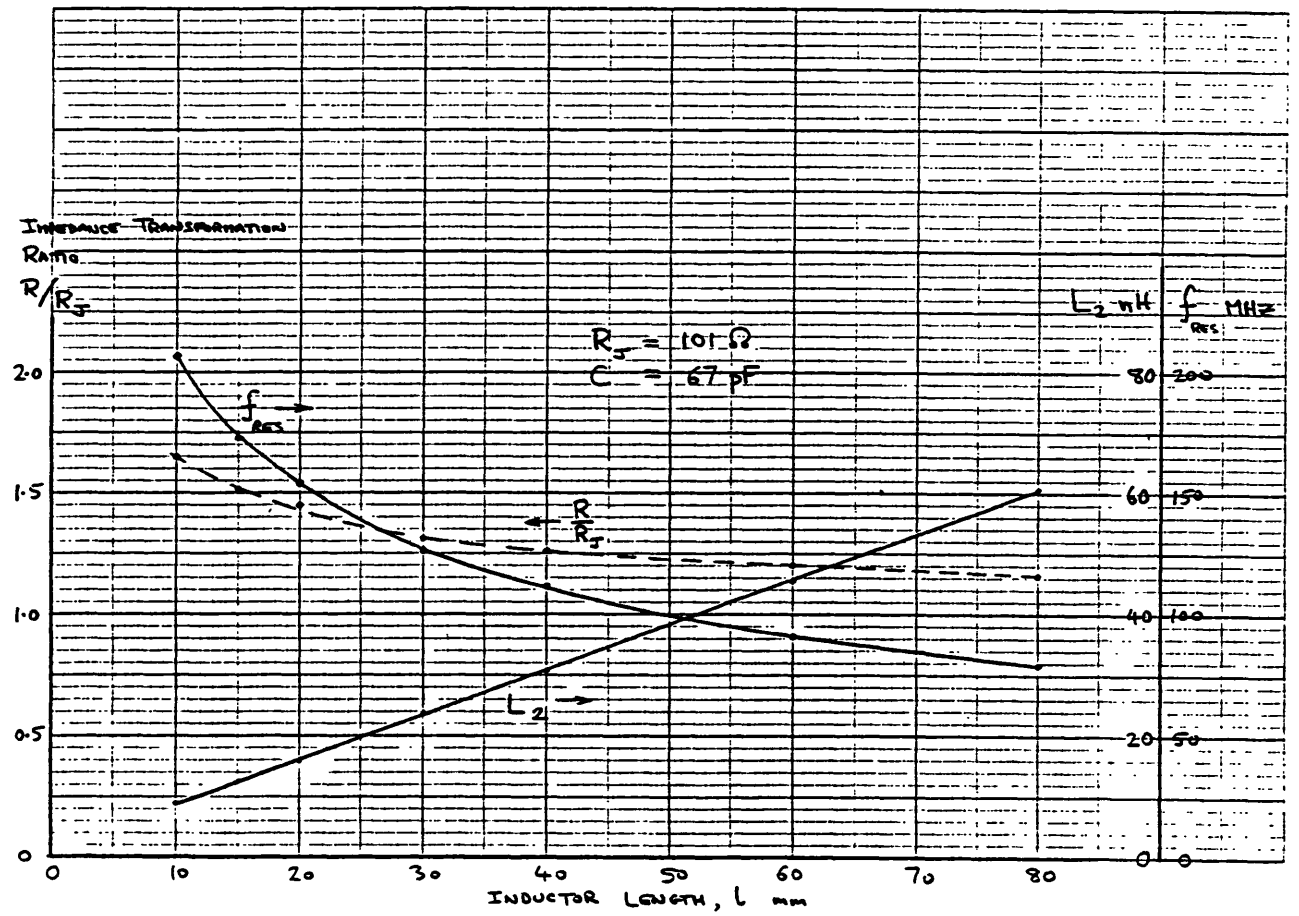

Fig. B-10 Impedance transformation ratio for the circuit of Fig. B-9(a) as a function of loop length, l. Also shown are the values of loop inductance, L_2, and resonant frequency for the particular element values used.

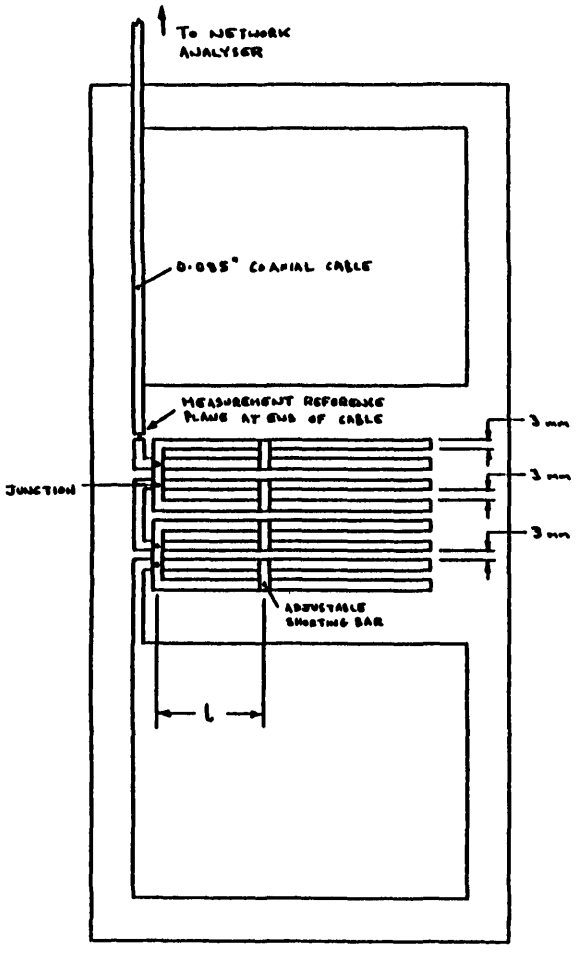

(a)

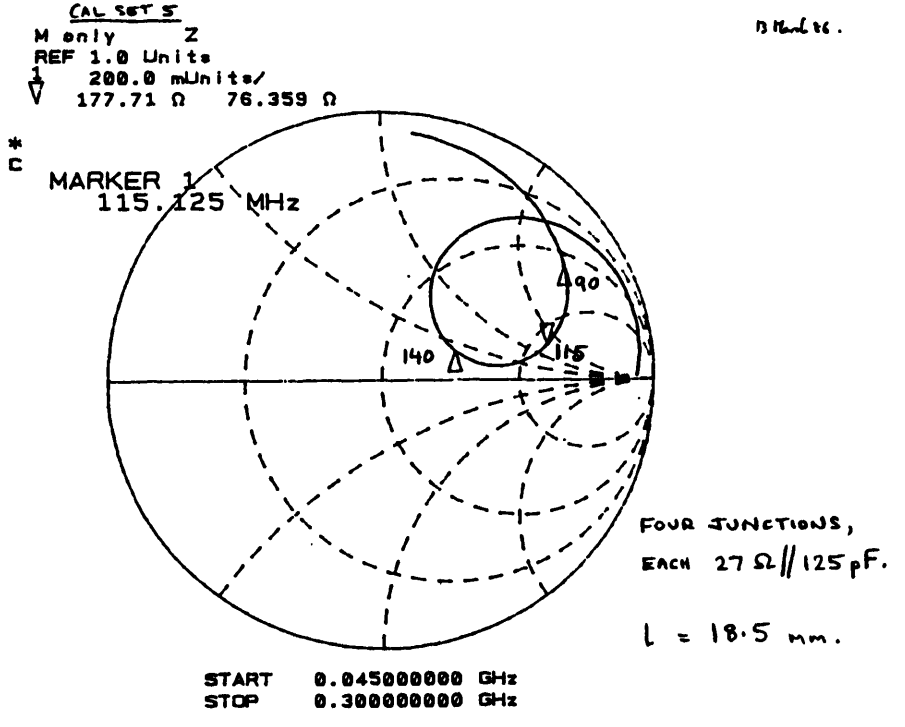

(b)

Fig. B-11(a) 1000 x scale model of a series array of four inductively tuned four-terminal junctions.

Fig. B-11(b) Measured impedance vs. frequency for the circuit of (a).

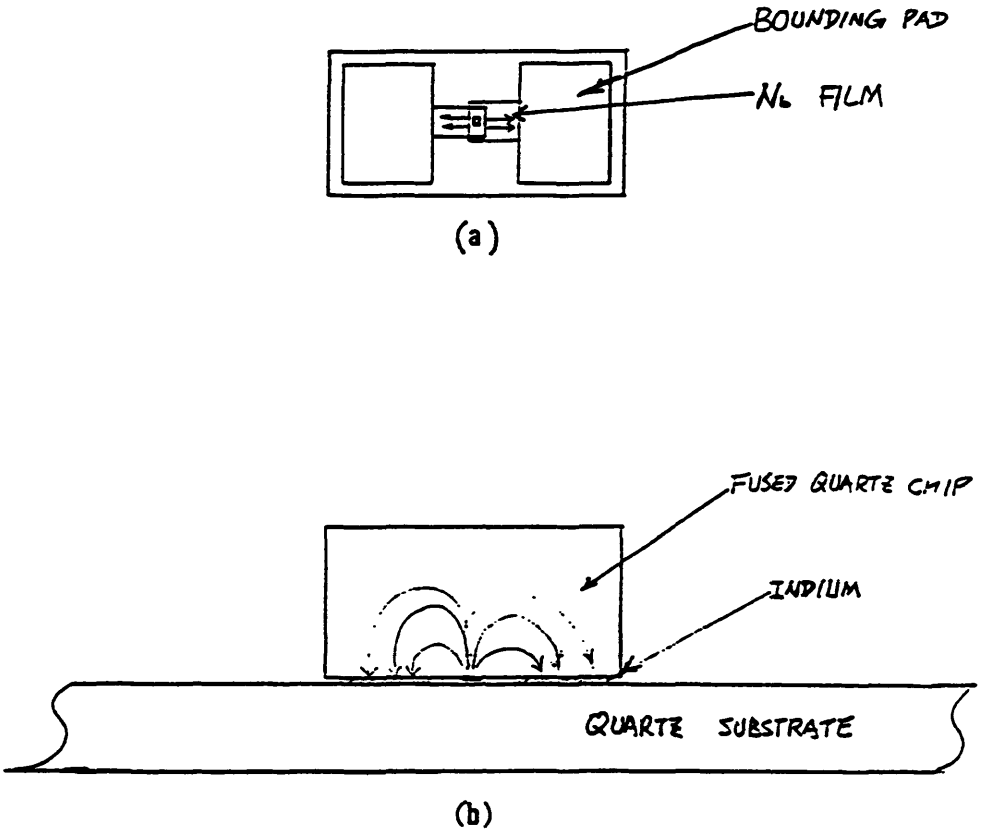

Fig. C-1. Thermal conduction paths of the SIS junction: (a) through the niobium thin film, and (b) through the fused quartz chip.

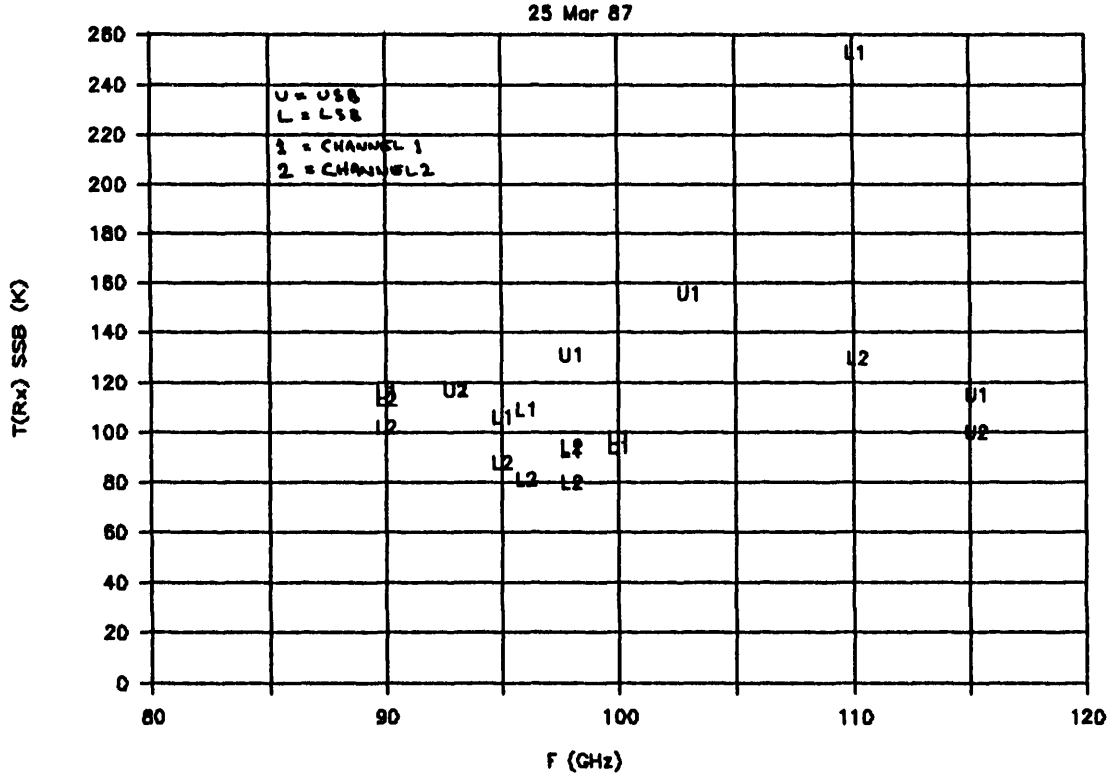

Fig. D-1. Single sideband noise temperature of the receiver on the 12-m Kitt Peak radio telescope. (Note that this is not the laboratory test receiver described in section II of this report). Numerals 1 and 2 identify the separate receiver channels. Characters U and L indicate operation in the upper or lower sideband. The receiver is normally operated in the single sideband mode with the tuning adjusted to reject the image sideband by at least 20 dB. The increase in receiver noise temperature near 110 GHz is believed to be a result of having insufficient LO power in this range.

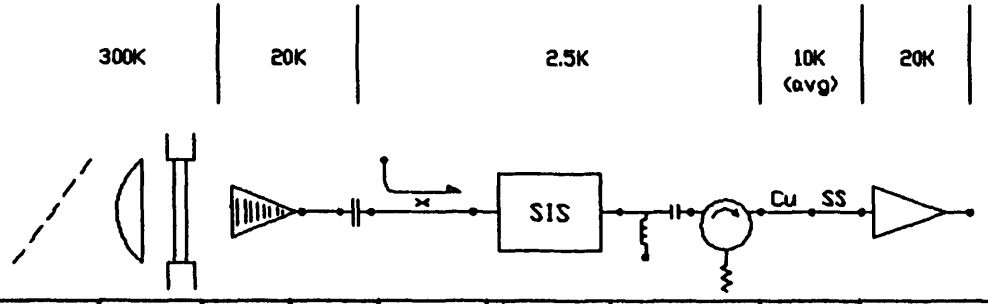

	Pol'n Splitter	Lens & Window	Horn	V/G & Gap	LO Coupler	Mixer	Bias-T Isol.	Cables	IF Amp.
Loss	0.15dB	0.20dB	0.05dB	0.48dB	0.38dB	4.96dB	0.30dB	0.20dB	
Tn	10.5K	14.1K	0.2K	2.3K	0.2K	20.5K	0.2K	0.5K	10K
Insert. Contrib. to Tr	14.3K	18.3K	1.2K	10.7K	6.8K	61.3K	4.0K	4.2K	47K
Tr	106K	92K	74K	73K	63K	58K	12K	11K	10K

Fig. D-2. Noise analysis of the telescope receiver. T_n is the individual noise temperature of each component, referred to its own input. The "Insertion Contribution to T_R" gives the effect on T_R of removing an individual component. Because the loss of each component multiplies the noise contributions of all following components, the sum of the insertion contributions is not equal to T_R for the whole receiver. The T_R values are the noise temperatures that would be measured if all components to the left of a particular point were removed.